Distinct endocytic pathways identified in tobacco pollen tubes using charged nanogold

Alessandra Moscatelli[1,*], Fabrizio Ciampolini[2], Simona Rodighiero[3], Elisabetta Onelli[1], Mauro Cresti[2], Nadia Santo[4] and Aurora Idilli[1]

[1]Dipartimento di Biologia L. Gorini, Università degli Studi di Milano, Via Celoria 26, 20133 Milan, Italy
[2]Dipartimento di Scienze Ambientali G. Sarfatti, Università degli Studi di Siena, Via P. A. Mattioli 4, 53100 Siena, Italy
[3]CIMAINA and [4]CIMA, Università degli Studi di Milano, Via Celoria 16, 20133 Milan, Italy
*Author for correspondence (e-mail: alessandra.moscatelli@unimi.it)

Accepted 9 August 2007
Journal of Cell Science 120, 3804-3819 Published by The Company of Biologists 2007
doi:10.1242/jcs.012138

Summary

In an attempt to dissect endocytosis in *Nicotiana tabacum* L. pollen tubes, two different probes – positively or negatively charged nanogold – were employed. The destiny of internalized plasma membrane domains, carrying negatively or positively charged residues, was followed at the ultrastructural level and revealed distinct endocytic pathways. Time-course experiments and electron microscopy showed internalization of subapical plasma-membrane domains that were mainly recycled to the secretory pathway through the Golgi apparatus and a second mainly degradative pathway involving plasma membrane retrieval at the tip. In vivo time-lapse experiments using FM4-64 combined with quantitative analysis confirmed the existence of distinct internalization regions. Ikarugamycin, an inhibitor of clathrin-dependent endocytosis, allowed us to further dissect the endocytic process: electron microscopy and time-lapse studies suggested that clathrin-dependent endocytosis occurs in the tip and subapical regions, because recycling of positively charged nanogold to the Golgi bodies and the consignment of negatively charged nanogold to vacuoles were affected. However, intact positively charged-nanogold transport to vacuoles supports the idea that an endocytic pathway that does not require clathrin is also present in pollen tubes.

Supplementary material available online at
http://jcs.biologists.org/cgi/content/full/120/21/3804/DC1

Key words: *Nicotiana tabacum* (L.), Pollen tube, Endocytosis

Introduction

During differentiation, plant cells translate external stimuli into peculiar differentiation patterns depending on tissue specificity. During this process, cells acquire different morphologies, typically by delivering new plasma membrane (PM) and cell wall material through the exocytotic pathway; a process that involves endoplasmic reticulum (ER) and dictyosome activity (Hepler et al., 2001). Besides an increase in cell volume, this process provides specific sets of proteins for the cell wall and PM depending on the differentiation pattern (Baluska et al., 2003). A polarized protein/lipid composition of the PM also implies selective removal/recycling of molecules regulating the polarity of cells and plant development, such as members of the PIN family of auxin efflux regulators and ion transporters between different PM domains (for a review, see Geldner and Jurgens, 2006). Polarity also requires internalization of PM segments, a process known as endocytosis in eukaryotic cells. In addition, to generate specific patterns of PM protein composition, endocytosis is involved in recycling excess secreted PM in cells with high secretory activity (Murphy et al., 2005). This process is especially significant for highly specialized cells such as pollen tubes, which grow only at the apex by an extreme form of polar growth, known as tip growth (Hepler et al., 2001). By this mechanism, post-Golgi secretory vesicles (SVs) are targeted and fuse with a restricted area of the apical PM (Steer and Steer, 1989), defining a tip-growth domain with a specific protein/lipid composition (Hepler et al., 2001; Kost et al., 1999; Potocky et al., 2003; Helling et al., 2006). During pollen tube growth, the high level of fusion of SVs largely exceeds PM extension (Steer and Steer, 1989; Derksen et al., 1995), so that an active mechanism of PM retrieval has been hypothesized to regulate the membrane economy of the cell.

In animal systems, besides the well-characterized clathrin-dependent endocytosis, clathrin-independent pathways have also been identified (Nichols and Lippincott-Schwartz, 2001) and shown to coexist in the same cell (Kirkham et al., 2005). In plants, only clathrin-dependent endocytosis has been described at the ultrastructural level in protoplasts using cationized ferritin and heavy metals (Tanchak et al., 1984; Fowke et al., 1991; Low and Chandra, 1994). Time-course analysis showed a degradation pathway by which the markers were first internalized in clathrin-coated vesicles at the PM and then delivered to partially coated reticulum, multivesicular bodies (MVBs) and finally to vacuoles. Plant partially coated reticulum was described as a system of interconnected tubular membranes; its morphological appearance suggested that it was similar to the recycling compartment described in animals (Hillmer et al., 1988; Geldner, 2004). Although endocytic compartments have been characterized unequivocally in animal cells and yeast (Gruenberg, 2001; Zerial and McBride, 2001), a full composition/functional description of plant endosomes is not yet available (Geldner, 2004; Geldner and Jurgens, 2006). Compartments of the trans-Golgi network

(TGN) were also recently identified as early endosomes (EEs) in plants (Dettmer et al., 2006), leading to the formulation of a new model, according to which early endosomal compartments and SVs meet in the TGN, which has been postulated as the first sorting station of endocytosis in plants (Dettmer et al., 2006). A sequence coding for a clathrin heavy chain (CHC)-like polypeptide was identified in soybean (Blackbourn and Jackson, 1996), and immunofluorescence studies (Blackbourn and Jackson, 1996) and observation of coated vesicles in the tip region (Derksen et al., 1995) suggests that a mechanism of clathrin-dependent endocytosis occurs in pollen tubes.

The endocytic process in pollen tubes of several species has recently been analyzed (Parton et al., 2001) by using FM4-64 (Bolte et al., 2004). This approach showed that, in pollen tubes, internalized PM was accumulated at the tip, in which a typical V-shaped fluorescent region was observed, suggesting that most of the internalized PM was redirected into the secretory pathway. However, because this probe inserts homogeneously into the PM, it shows the endocytic process as a whole but does not provide information about different endocytic modes that might occur in pollen tubes.

In an effort to identify different internalization pathways, positively or negatively charged nanogold (Prescianotto-Baschong and Riezmann, 1998) was used in tobacco pollen tubes. Positively or negatively charged nanogold particles bind negatively or positively charged residues on the PM, respectively, showing the fate of internalized PM segments in different regions at the ultrastructural level. Time-course experiments showed that distinct areas of endocytosis occur in pollen tubes. Positively charged nanogold revealed an endocytic pathway that involved subapical PM domains that, after internalization, were mostly recycled in the secretory pathway, presumably through the Golgi apparatus and to the smooth ER. Two degradative routes were shown by positively and negatively charged nanogold pattern distribution. Both probes followed the degradation pathway, probably involving elements of the TGN and leading to MVBs and vacuoles. However, only a minor amount of the positively charged nanogold was delivered to vacuoles, whereas most of the negatively charged nanogold followed the degradation route.

Ikarugamycin (Ika), an inhibitor of the clathrin-dependent endocytosis in animal cells, was used to dissect the endocytic pathway in pollen tubes (Hasumi et al., 1992; Luo et al., 2001). Ika affected internalization in the apical and subapical regions, leading to the partial inhibition of the PM recycling into the Golgi/secretory pathway. Electron microscopy showed that Golgi bodies were hardly stained by the positively charged nanogold in the presence of Ika, whereas the degradative pathway did not seem to be affected, suggesting that clathrin-dependent and -independent endocytosis both occur in pollen tubes.

Results

Time-course experiments

In order to distinguish endocytic pathways involved in PM recycling and/or remodelling during pollen tube elongation, positively and negatively charged nanogold was used. Because of the nature of these probes, which interact with PM molecules on the basis of opposite ionic charges, we could not exclude that either could show more than one internalization pattern or that their patterns could partially overlap. Nanogold is reported to be relatively small (1.5-1.6 μm) and the presence of the probe requires a procedure of silver enhancement in order to be observed as dark spots. This gold core is functionalized with a layer of organic ligands bound to the surface of the gold atoms, such as several primary amine groups and multiple carboxylic acidic groups for positively and negatively charged nanogold, respectively. In order to determine the real diameter of the probes, electron microscopy (EM) observations were carried out to measure the size of the positively and negatively charged nanogold (see particles in supplementary material Fig. S2a-b′). The size of the particles was variable, mostly ranging from 1.29-1.89 and 1.29-1.60 μm for positively and negatively charged nanoparticles, respectively (supplementary material Fig. S2a-b′)

An intrinsic difficulty in analyzing samples was due to pollen tube length. To evaluate the distance from the apex of the observed areas we needed sections showing the whole cell, which was very difficult because of tube length. However, the polarized structure of pollen tubes, which accumulate SVs at the very tip (3-5 μm from the apical PM) and maintain larger organelles in regions progressively distant from the apex, allowed us to establish at least approximately how far from the tip we were making observations. Preliminary experiments and quantitative analysis were performed in order to exclude that these probes affected pollen viability and tube elongation. Incubation with positively or negatively charged nanogold did not significantly influence tube growth (Fig. 1a,b). However, after 2 hours incubation, the presence of positively charged nanogold seemed to slightly enhance the pollen tube growth rate, whereas negatively charged nanogold did the contrary, slightly inhibiting tube growth. Nevertheless, the fluorescein diacetate (FDA) (Heslop-Harrison and Heslop-Harrison, 1970) assays showed that pollen viability was maintained during the experiment in the presence of these probes (data not shown).

Positively charged nanogold internalization revealed a major PM recycling into the secretory pathway involving the Golgi apparatus and a minor degradative pathway

Vesicle-mediated internalization of positively charged nanogold was observed in subapical regions, presumably in the organelle-rich zone, starting about 5-10 μm beyond the very tip after 30 minutes of incubation (Fig. 2a). Nanogold particles regularly associated with the PM were trapped inside invaginating PM segments (Fig. 2a, arrowhead) and within vesicles just below the PM surface (Fig. 2a, red asterisks), probably representing recently invaginated vesicles/endosomes. In regions progressively distant from the cell surface, small vesicles seemed to contain the probe (Fig. 2a, black arrows), probably representing EE compartments to which the internalized nanogold is consigned and sorted for further processing, or, alternatively, functioning as elements involved in trafficking among different membrane compartments. At this time, other membranous organelles participate in the endocytic process; labelled vesicles closely related to the trans face of the Golgi complex (Fig. 2a, yellow arrows) and the rims of cis and medial cisternae (Fig. 2a, indicated with G, blue arrowhead, and Fig. 2b, blue arrowheads) suggested that dictyosomes could be involved early in the endocytic pathway. Vesicles containing electron-dense material similar to that observed in the cell wall, outside

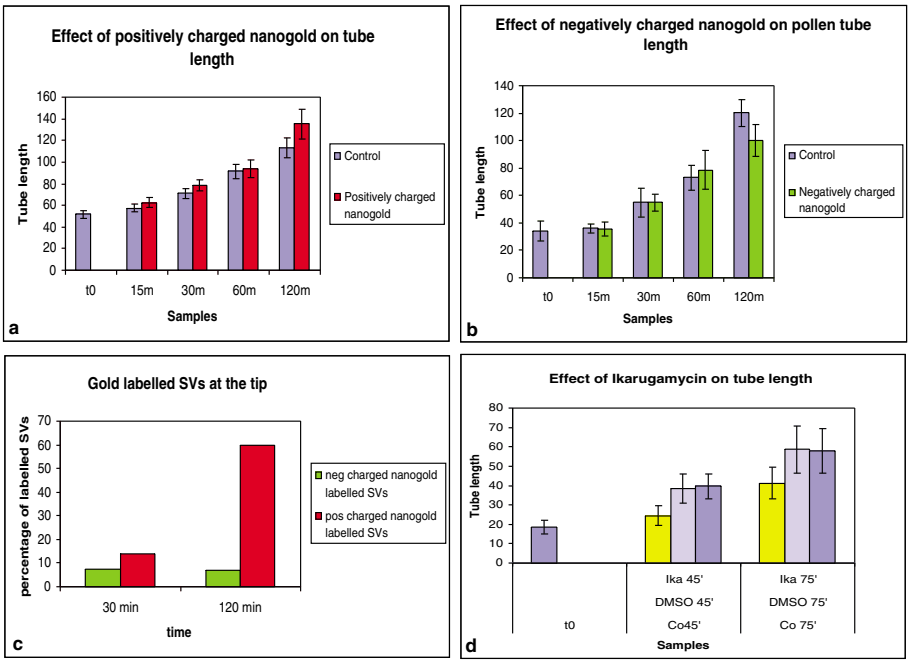

Fig. 1. (a,b) Tube lengths with and without probes were compared. Probes do not significantly influence tube length. *x* axis shows time in minutes (m). (c) Percentage of stained vesicles in the tips of pollen tubes incubated with negatively or positively charged nanogold. (d) Pollen tube growth in the presence of Ika (yellow bars) was compared with tubes grown in control medium (dark-purple bars) or in medium containing the Ika solvent (DMSO) (light-purple bars). Error bars indicate 95% confidence intervals (n=100-140).

the PM, were also involved in nanogold internalization (Fig. 2c, see arrowhead), suggesting that endocytosis could play a role in regulating cell wall composition/recycling. Structures morphologically similar to MVBs also appear to be labelled at this time (Fig. 2d), showing that positively charged nanogold at least partially followed the degradation pathway. On rare occasions, gold particles could be observed in vesicles in the tip region after 30 minutes of incubation (Fig. 2e), suggesting that internalization of positively charged nanogold does not occur in this region and that the faintly labelled vesicles (Fig. 2e, red asterisks) could represent early recycling of PM regions to the secretory pathway. In subapical regions, a large amount of binding of positively charged nanogold with the cell wall was observed (Fig. 2g). In contrast to what was observed in subapical regions, in the clear zone of the tubes the association of positively charged nanogold with the cell wall was less conspicuous (Fig. 2e), in line with the presence of pectins being secreted only in the their esterified form in this region (Bosch and Hepler, 2005). Regularly spaced gold particles were seen on the PM surface (Fig. 2f,g) with increasing distance from the apex, but internalization events were not observed in these areas. After 15 minutes, no positively charged nanogold particles were seen in the cytoplasm (not shown).

After 1 hour, the gold distribution pattern was similar to that observed after 30 minutes. Only occasionally were particles seen in small vacuole-like compartments (Fig. 3a,b), suggesting that the degradative pathway was not prevalent. After 2 hours, the distribution of positively charged nanogold closely resembled that already described at 30 minutes and 1 hour. Staining was observed at the PM and in invaginating vesicles (Fig. 3c, arrow) and in vesicles in the cortical region of the cytoplasm (Fig. 3c). Positively charged nanogold decorated Golgi cisternae and vesicles associated with the cis, medial and trans faces of Golgi bodies (Fig. 3d). The labelling of Golgi bodies was a constant feature of cells after positively charged nanogold internalization: 14 dictyosomes of the 16 found were labelled, suggesting that a substantial amount of internalized PM, which binds positively charged nanogold, could be recycled to the secretory pathway. This hypothesis was further supported by the accumulation of gold particles in vesicles in the clear zone of the tubes after 2 hours of incubation (Fig. 3e). Careful observation of the apical zones showed staining associated with the PM surface. This could further confirm the hypothesis that most internalized PM could be conveyed to the apex via the secretory pathway (Fig. 3e). Stained elements of smooth ER containing gold particles were frequently observed in the tip region among the SVs, sometimes in close contiguity with them (Fig. 3e, arrows). Quantitative analysis of stained SVs at the tip in EM micrographs suggested an increase in stained SVs between 30 minutes and 2 hours (Fig. 1c). The above results suggest that endocytosis could be involved in maintaining the cell membrane economy in pollen tubes, because most internalized PM is re-used in the process of secretion for the tip growth. In order to observe whether gold particles accumulated in certain membranous compartments, pulse-chase experiments were performed. Cells were incubated with the probe for 30 minutes and then gold particles were removed from the medium. Pollen tubes grew for a further 30 minutes in gold-free medium. After this time, positively charged nanogold particles were occasionally found in the lumen of vacuoles (Fig. 4a), but other cytoplasmic areas did not show labelled compartments (Fig. 4b).

In order to exclude the possibility that the gold labelling described above is an artefact due to aspecific silver precipitation, sections of pollen tubes not previously incubated with the probes were processed for silver enhancement. Rare gold particles were occasionally observed on the cell wall of the granule (supplementary material Fig. S1Ab), but no staining was seen in the cytoplasm (supplementary material Fig. S1Aa,c).

Negatively charged nanogold revealed an internalization pattern at the very tip and showed an endocytic route primarily directed to vacuoles

Similar time-course experiments were performed using negatively charged nanogold. Observation of samples taken at the same times showed that internalized PM segments followed a distinct endocytic pathway and timing, because, after 15 minutes of incubation, nanogold particles were already found in vesicles associated with the trans face of the Golgi apparatus (Fig. 5a, arrows); these vesicles seemed to be closely associated with a vacuole-like compartment into which nanogold particles were released (Fig. 5a, arrowheads). In other images, the probe was in vacuoles containing electron-dense material (Fig. 5b, arrows); here, gold particles were not associated with the vacuole membrane but were in the lumen of the organelle.

Gold uptake could be observed in the clear zone in sections of cells after 30 minutes of incubation. In Fig. 5c (arrowhead), the probe decorated a small number of vesicles at the apex; gold particles were frequently associated with the cell wall and PM surface in regions just behind the tip (Fig. 5d) but vesicle-mediated internalization of PM with negatively charged nanogold bound to it was not observed, suggesting the presence of distinct internalization zones for positively and negatively charged nanogold. In contrast to what we observed with positively charged nanogold, none of the other membranous organelles, such as smooth ER or Golgi cisternae, appeared to be labelled by the probe at this time (Fig. 5d,e). After 1 hour, sections of the apical regions showed association of probe with the PM surface and particles were also seen in vesicles, very close to the PM (Fig. 6a, arrows). In areas progressively distant from the tip, negatively charged nanogold was associated with the outer surface of the PM (Fig. 6b,c,e); only rarely were gold particles found in vesicles and they were never observed in membranous organelles such as the ER or Golgi bodies (Fig. 6b,e,f). After 2 hours, a limited number of labelled vesicles was observed at the tip (Fig. 7b), but the probe did not accumulate in this region, because the percentage of labelled vesicles remained constant between 30 minutes and 2 hours (Fig. 1c). Gold particles were not observed in Golgi bodies or ER in apical or subapical regions (Fig. 7b,c).

In our observations of pollen tubes incubated with negatively charged nanogold, we found 12 sections of dictyosomes: none were labelled by the probe except for vesicular-tubular elements connected with the trans face of the

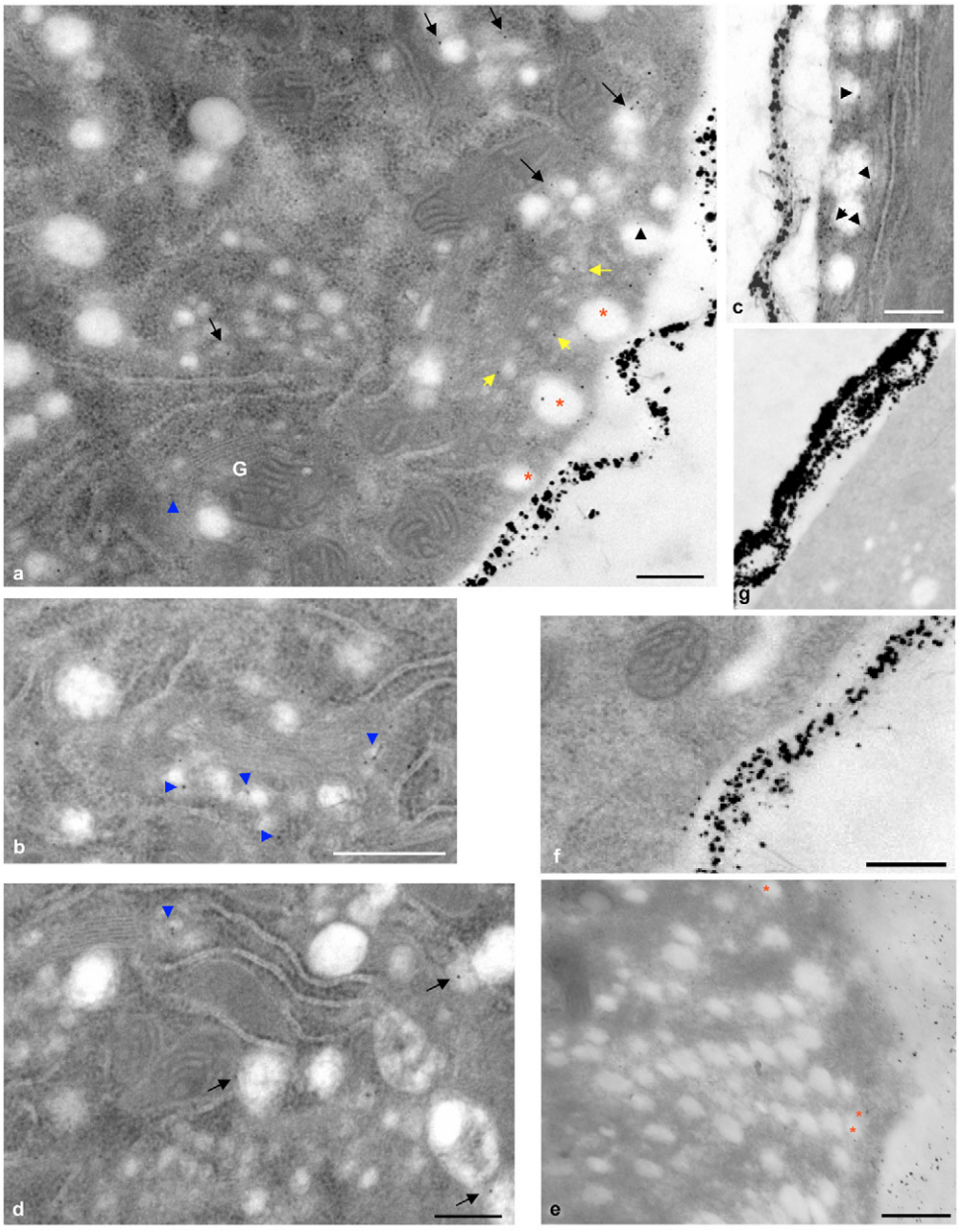

Fig. 2. Internalization of positively charged nanogold for 30 minutes. (a) After 30 minutes, positively charged nanogold (black dots) was regularly distributed on the PM and was trapped in invaginating vesicles (black arrowhead) and in vesicles immediately beneath the PM (asterisks). Vesicles of the TGN were stained (yellow arrows) as well as vesicles associated with the cis and medial rims of Golgi cisternae (G, blue arrowhead). Black arrows indicate labelled cytoplasmic vesicles. (b) A Golgi apparatus showing labelled vesicles associated with cis and medial cisternae (arrowheads). (c) Gold particles were internalized in vesicles containing cell wall components (arrowheads). (d) MVB-like compartments were labelled (arrows) as well as Golgi body vesicles (blue arrowhead). (e) A tip region showing a few stained vesicles (asterisks). (f,g) Regions far from the tip showing gold particles (black) regularly spaced on the PM surface. Bars, 0.5 μm (a,b,d-g), 1 μm (c).

Golgi bodies (Fig. 5a). Although particles were often associated with the PM surface in regions far from the apex (Fig. 7a), it is unlikely that this represents a step preceding the uptake of the probe, because no vesicles containing gold particles were seen immediately under the labelled PM. A number of labelled compartments, morphologically similar to vacuoles, were observed in the tubes (Fig. 7d), confirming the idea that negatively charged particles transported far from the tip region could be on the degradation pathway.

Taken together, these observations revealed that internalized PM binding negatively charged nanogold follows a distinct endocytic pathway with respect to that binding positively charged nanogold. The frequent labelling of vacuole-like compartments by negatively charged nanogold suggested that this pathway could be the main degradation pathway of pollen tubes. Alternatively, after internalization in the tip region, part of the vesicles might be reinserted in the tip PM without involving the Golgi-dependent secretory pathway. In this respect, pulse-chase experiments carried out using negatively charged nanogold showed that these particles persisted in vesicles in the tip region 30 minutes after probe removal (Fig. 4c), suggesting that recycling of endocytic vesicles was limited to the tip region. Furthermore, because a large number of vacuoles were stained by negatively charged nanogold after pulse-chase experiments (Fig. 4d), these vesicles could be considered the final destination of this probe.

In vivo FM4-64 uptake confirmed the presence of two internalization regions

In time-lapse experiments, growing pollen tubes were incubated with 1 μM FM4-64 and cells were recorded for at least 300 seconds in order to analyze the manner of the probe uptake in different regions of the tube. Quantitative analysis of internalization was performed in the extreme 5 μm of the tip [Fig. 8Aa-a″, see the green region of interest (ROI)] and in the flanks (up to 30 μm from the apical PM; Fig. 8Aa-a″, violet and orange ROI, frames a-a″ are part of supplementary material Movie 1). Simultaneous uptake of FM4-64 was observed in the tip and subapical regions, being greater in the latter (Fig. 8Ab, supplementary material Movie 1). In order to validate the quantitative analysis and confirm the reproducibility of the results, statistical analysis of the data was performed considering six independent experiments of FM4-64 internalization; these results showed that endocytic activity in the subapical regions of the tube (5-30 μm from the very tip) was almost double that at the tip (5 μm from the apical PM) (Fig. 9Ab).

These findings were confirmed with the *t*-test, showing a *P* value of 0.01401 between fluorochrome entrance in the apical and subapical regions (Fig. 9). These results confirmed what was suggested by EM observations, namely that negatively charged nanogold was taken up by a relatively small number of vesicles in the tip region (Fig. 4), whereas positively charged nanogold was internalized in the subapical region, in which a large number of vesicles seemed to be involved in endocytosis (Fig. 2a,c and Fig. 3c). These data further support the idea that internalization events at the tip and in the subapical

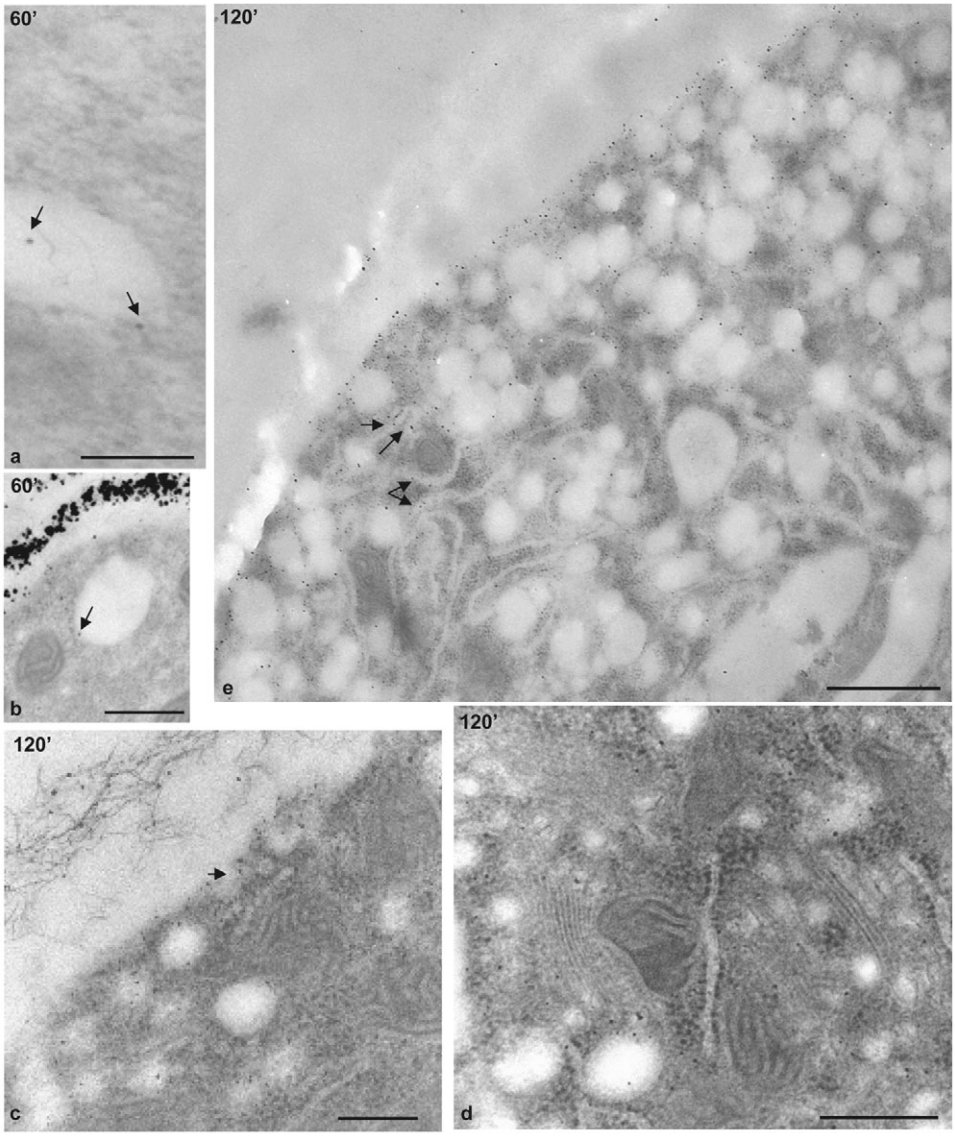

Fig. 3. Internalization of positively charged nanogold for 1-2 hours. (a,b) After 1 hour, vacuoles were labelled (arrows). (c) After 2 hours, gold uptake occurred in subapical regions of the tube (black arrow). (d) Gold particles in vesicles and cisternae of the cis, medial and trans faces of Golgi bodies. (e) A large number of stained vesicles were observed in the tip region. Gold particles were observed in tubules of smooth ER (arrows). Bars, 0.5 μm.

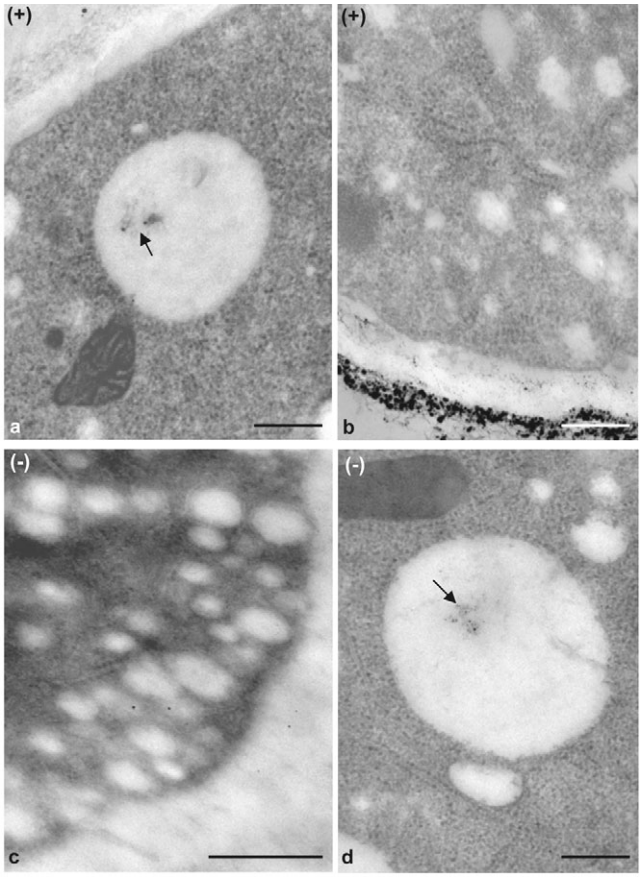

Fig. 4. Pulse chase using charged nanogold. (a,b) Positively charged nanogold (+) accumulated in vacuoles (arrow), but was not observed in other organelles. (c,d) Negatively charged nanogold (–) was found in vesicles in the tip region (c) and in vacuoles (d, arrow). Bars, 0.5 μm.

region could represent distinct endocytic pathways. They also suggest that vesicles accumulating at the tip, generally referred to as SVs, include many endocytic vesicles/endosomes.

In vivo pulse-chase experiments confirmed that internalized PM is reused for secretion, through the Golgi apparatus, and is partially destined to vacuoles

EM observations using charged nanogold suggested that internalized PM is partially reused for the exocytosis and also showed a degradative pathway leading to vacuoles. Pulse-chase experiments using FM4-64 were performed in order to confirm the presence of these pathways. Cells were observed at different times after fluorochrome loading (1 hour): FM4-64-labelled membranes form a typical V-shaped staining pattern at the tube tip 15 minutes after pulse (Fig. 10Aa,a′), confirming that most of the internalized PM was recycled to the apex, where Golgi-derived SVs are concentrated in order to be fused with the PM. The FM4-64 labelled membranes in the apex seemed to be dynamic, because images taken at intervals of 30 seconds, 15 minutes after pulse, showed different shapes of the apical fluorescence accumulation (Fig. 10A, compare images a′ and a″). Time-lapse analysis of the FM4-64 staining pattern in the tip region confirmed these observations and revealed that fluorescence accumulation was reoriented during changes of pollen tube growth direction (supplementary material Movie 2). Five hours later, the fluorescence in the apex, as well as in the apical PM, was faint, supporting the idea that most of the FM4-64-labelled apical vesicles fused with the PM for pollen tube elongation (Fig. 10Ab). These data confirm that internalized PM is largely reused for secretion, as suggested by the data of positively charged nanogold.

After 5 hours, the apex was deprived of staining, but labelled organelles were observed in the older regions of the tube in which vacuoles were usually present (not shown). In order to prove that membranes delimiting the acidic compartments were labelled by FM4-64, at 24 hours after pulse cells were incubated with the LysoSensor blue DND-167, a fluorescent pH indicator probe that accumulates, as the result of protonation, in acidic organelles. Vacuoles stained by the LysoSensor are shown as blue globules in the cytoplasm (Fig. 10Ab′) and analysis of colocalization showed a signal overlapping in vacuoles delimiting membranes (Fig. 10Ab″,b‴, see white spots and cytofluogram). Staining of vacuolar membranes 24 hours after pulse further supported the evidence obtained by the positively and negatively charged nanogold internalization, showing that degradative pathways act in pollen tubes.

Data of positively charged nanogold showed that Golgi bodies are involved in PM recycling. In order to confirm this observation, double labelling was performed in pollen tubes in vivo using BODIPY TR-Ceramide (Fig. 10, red), which produces a selective staining of the Golgi complex or of Golgi-derived vesicles and FM4-64 (Fig. 10, shown as green staining). The BODIPY TR-Ceramide-stained spots were dispersed in the cytoplasm and were more concentrated in the apical region (up to 20 μm from the apical PM), in which they were organized to form a collar-like structure in the apical region of the tube (Fig. 10Ba,b, arrows).

After loading with the BODIPY TR-Ceramide, pollen tubes were incubated with FM4-64 and images of colocalization were taken at different times. After 5 minutes, a partial colocalization was observed (Fig. 10Bc, see the cytofluogram) in the region of the collar-like structure shown by the BODIPY TR-Ceramide (Fig. 10Ba″, white spots), whereas, after 30 minutes, a more widespread colocalization was recorded (Fig. 10B,d, see the cytofluogram) in the apical region of the tube (Fig. 10Bb″, white spots), suggesting that part of the internalized PM was actually transported to the Golgi apparatus and then reused for the production of SVs.

To avoid crosstalk between the two probes, control experiments were performed in which pollen tubes were loaded with BODIPY TR-Ceramide only (supplementary material Fig. S1Ba,a′) and images were taken using the parameters used for the FM4-64. A very low level of background was observed (supplementary material Fig. S1Ba″), so artefacts were excluded.

Dissection of endocytosis using Ika revealed that clathrin-dependent endocytosis occurs in the apical and subapical regions

In order to characterize endocytic pathways in tobacco pollen tubes, Ika, an inhibitor of clathrin-dependent endocytosis, was used. Ika is known to inhibit the uptake of clathrin-dependent PM receptors in mammalian cells without affecting internal

trafficking (Hasumi et al., 1992; Luo et al., 2001). The effect of Ika was first tested by time-lapse experiments in live cells; pollen tubes were incubated with 3 μM Ika for 15 minutes before addition of the probe. Time-course analysis of FM4-64 internalization was performed using the same microscope setup in the presence of Ika and in control experiments observing medial sections of tubes. Observations were based on six pollen tubes. Fluorochrome internalization was measured in the same regions as reported in control tubes (Fig. 8Ba-a″, see green, violet and orange ROI at tip and flanks of tube at t^0 and after 151 and 320 seconds; frames a-a″ are part of supplementary material Movie 3).

Remarkably, FM4-64 immediately bound to the PM, but quantitative analysis, performed as described above for control experiments, revealed that although a small peak of fluorescence was often observed during internalization in the presence of Ika, the fluorescence intensity remained low with respect to the control (Fig. 8Bb). Images of the same pollen tube analyzed for fluorochrome internalization, taken after the addition of FM4-64, revealed that the process of endocytosis had not completely stopped, because fluorescent spots were observed in the cytoplasm after 30 minutes and 1 hour (Fig. 8Bc-e). During internalization experiments with Ika, accumulation of fluorescence was often observed in the subapical region of the PM (Fig. 8Bc-e, supplementary material Movie 3), presumably reflecting inhibition of PM internalization in this region. In line with this observation and with data derived from endocytosis of positively charged nanogold, accumulation of fluorescence at the tip was only seen in about 20% of treated pollen tubes, suggesting that Ika interfered with internalization of PM that was then recycled to the tip for tube growth. In control experiments, after 1 hour of incubation with FM4-64, all tubes displayed the usual V-shaped accumulation of probe in the apical dome (not shown).

Although a reduction in pollen tube length was observed with respect to control samples in the presence and absence of DMSO, Ika did not completely inhibit pollen tube growth after 45-75 minutes of incubation (Fig. 1d). Often we observed that a reduction in growth rate was accompanied by tip swelling (Fig. 8Bc′-e′). Measures of fluorochrome internalization in the presence of Ika were compared with those of control experiments (Fig. 9Ab); in the presence of Ika, the difference in the amount of FM4-64 internalization in the apical versus subapical regions of the tube was reduced (Fig. 9Ab) so that the *t*-test gave a *P* value of >0.05 (Fig. 9). When we compared entrance of FM4-64 in the apical regions in the presence and absence of Ika, we observed that Ika induced a significant reduction in uptake (P=0.01) (Fig. 9). This reduction was enhanced when the same analysis was carried out comparing the fluorochrome uptake in the subapical regions in the presence and absence of the drug. In the latter case, the *t*-test gave a *P* value of 0.001, suggesting that clathrin-dependent endocytosis is also elevated in the subapical domes of the tubes (Fig. 9).

These results led us to postulate that

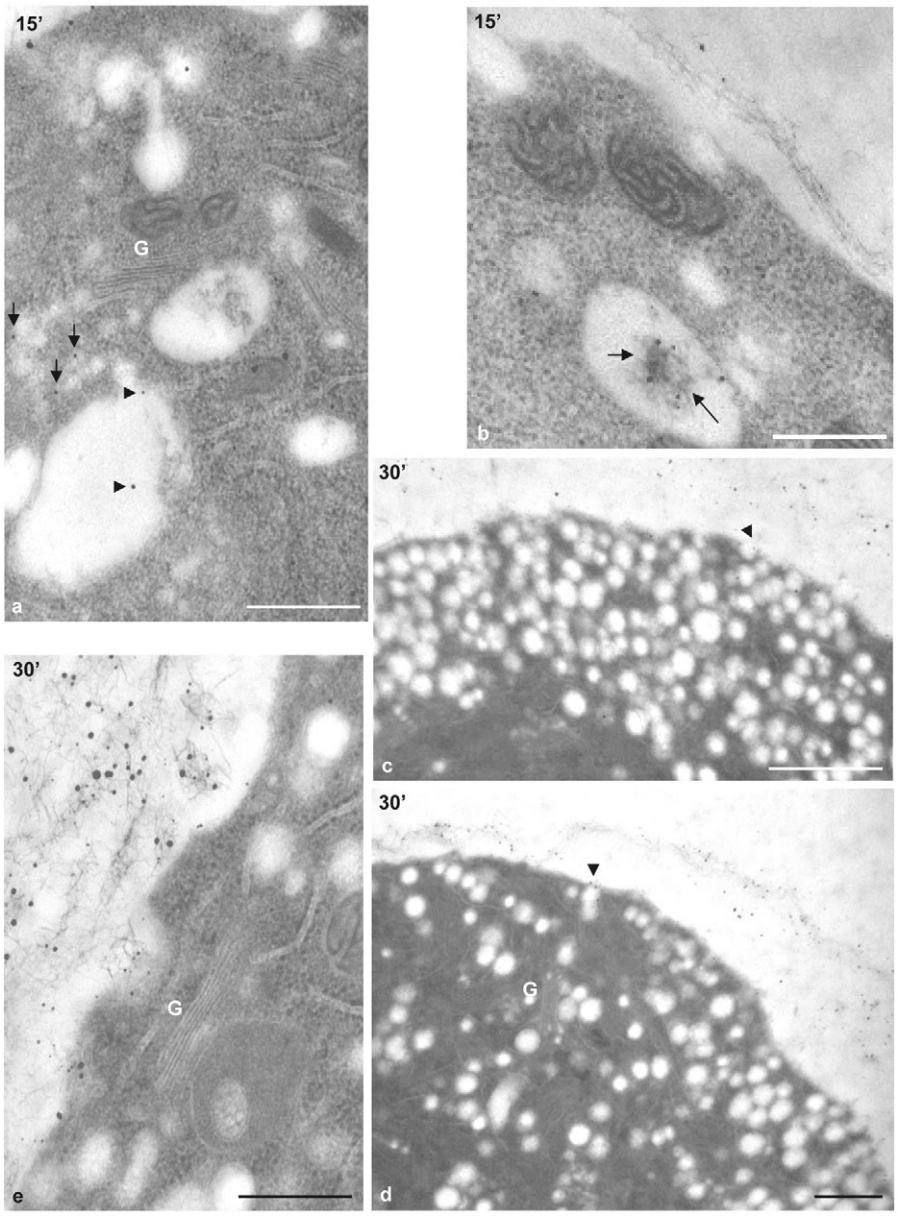

Fig. 5. Internalization of negatively charged nanogold for 15-30 minutes. (a,b) After 15 minutes, negatively charged nanogold was seen in vesicles in the TGN region (a, arrows) and in vacuole-like compartments (a, arrowheads and b, arrows). (c) After 30 minutes, invaginating vesicles were seen in the tip (arrowhead), whereas few vesicles were labelled in the apex. (d) No internalization was observed in the subapical region of the tube and Golgi (G) bodies were not labelled. Arrowhead indicates gold particles on the PM in the organelle-rich zone. (e) Organelle-rich zone showing unlabelled Golgi apparatus (G). Bars, 0.5 μm (a,b,e), 1 μm (c,d).

clathrin-dependent endocytosis was involved in internalization of PM at the apex and in the subapical regions of pollen tubes, but because inhibition was not complete, that clathrin-independent pathways could also play a role in growing pollen tubes. To better understand which internalization patterns were inhibited, EM observations of pollen tubes were made after internalization of charged nanogold in the presence of 3 μM Ika.

In the presence of Ika, positively charged nanogold was observed in vacuoles with a frequency similar to that of the control (Fig. 11a,b, arrows), whereas Golgi bodies were hardly stained (Fig. 11b, Golgi is indicated with G). In our observations (ten Golgi bodies were observed), we only found labelled vesicles adjacent to the rims of Golgi cisternae after 60 minutes of incubation in one case (Fig. 11d, blue arrows), whereas the other Golgi bodies did not show gold particles (Fig. 11b) or only vesicles associated with the TGN were labelled (Fig. 11d, yellow arrow). However, internalization events still occurred in the organelle-rich zone of the tube (Fig. 11d, black arrowheads); nanogold particles were also observed in vesicles under the PM, deeper in the cytoplasm (Fig. 11c, arrowheads) and in large vesicles/endosomes (Fig. 11d, red asterisks), as observed in control experiments (Fig. 2a). Vesicles containing fibrillar material also contained gold particles, suggesting that clathrin-independent endocytosis could be responsible for cell wall remodelling and internalization of PM for degradation, whereas Ika mostly seemed to affect internalization of PM domains that were recycled to the secretory pathway. Negatively charged nanogold was only rarely observed in vesicles/endosomes in the presence of Ika (Fig. 11f, arrowhead) but it was never observed in vacuoles or other organelles (Fig. 11e,g), suggesting that internalization of PM domains for degradation occurs by different mechanisms.

Effect of Ika on the distribution of CHC in pollen tubes

In order to investigate how Ika could inhibit clathrin-dependent endocytosis, we performed immunolabelling experiments to see whether this drug affected clathrin distribution in pollen tubes. The specificity of the anti-CHC monoclonal antibody 4A8 (Blackbourn and Jackson, 1996) was tested on tobacco pollen tube crude extract and the antibody identified a single polypeptide with a molecular weight of 167 kDa (Fig. 12A, arrow). Pollen tubes grown in control medium and medium supplemented with 3 μM Ika were processed for immunostaining. Medial sections (1 μm) of treated pollen tubes showed fluorescent staining presumed to be associated with the PM in the apical and subapical regions after 15 (Fig. 12Ba,a′) and 45 (Fig. 12Bb,b′) minutes of incubation with the drug, whereas, in pollen tubes maintained in control medium, punctate staining was observed on the PM surface (Fig. 12Bc,c′, arrowheads) and in the cytoplasm, suggesting that Ika

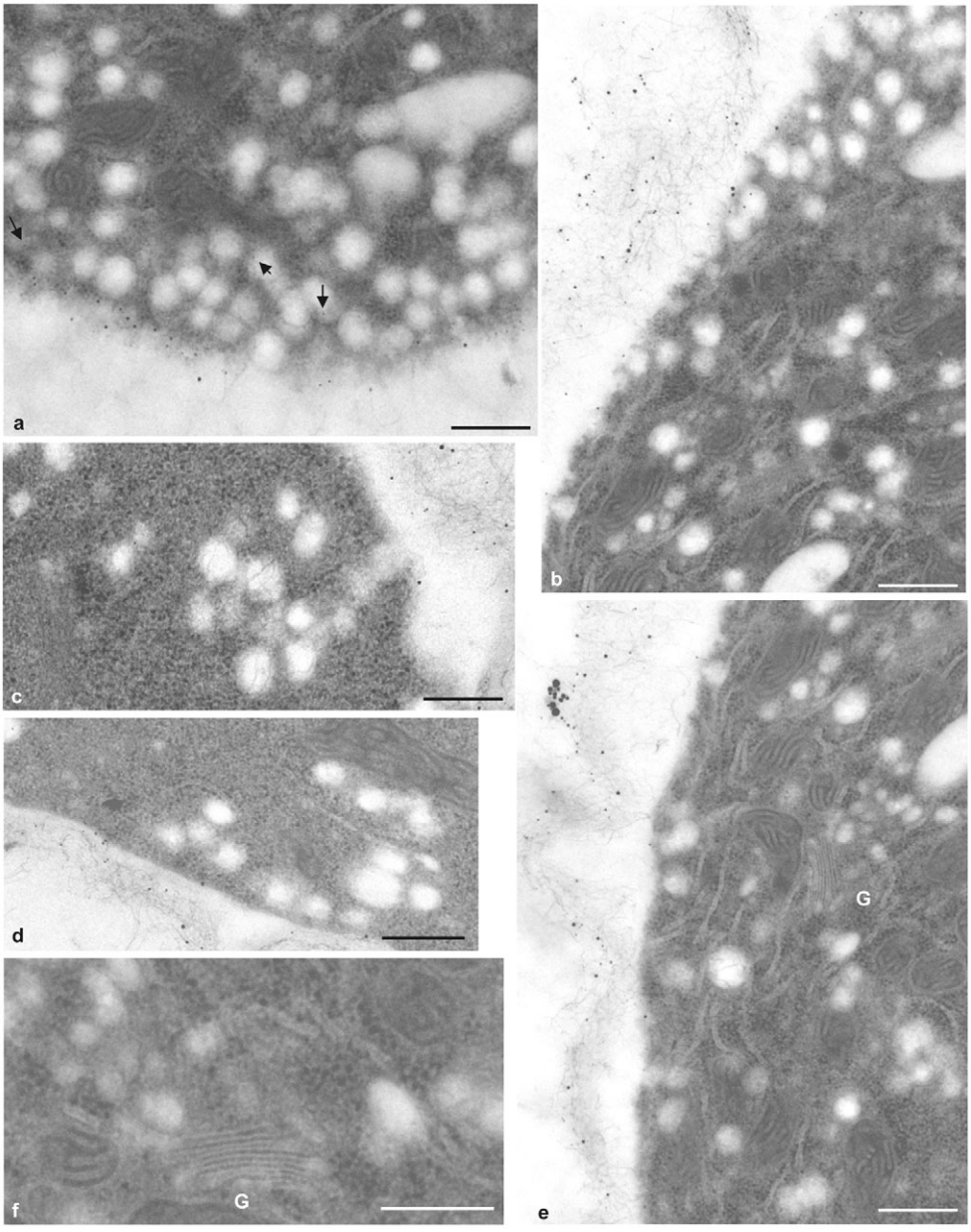

Fig. 6. Internalization of negatively charged nanogold for 1 hour.
(a) Accumulation of probe was not observed in the tip region, in which a limited number of vesicles was labelled (arrows).
(b-e) Internalization was not observed in the subapical region (b-d) or in the region far from the tip (e).
(b,d,f) Negatively charged nanogold was never observed within membranous organelles such as the ER or Golgi bodies (G). Bars, 0.5 μm (a-e), 1 μm (f).

does indeed affect clathrin distribution in pollen tubes, possibly by inhibiting the pinching off of clathrin-coated vesicles at the PM.

In order to confirm that Ika increased the association of CHC with the PM, microsomes were prepared from pollen tubes grown with or without 3 μM Ika. In the presence of the drug, an increase in the amount of CHC associated with the microsome fraction (P2) was observed with respect to the soluble fraction (S2) (Fig. 12C, 3 μM Ika, upper blot). Densitometric analysis on western blot membranes after labelling with 4A8 antibody showed that, in pollen tubes incubated for 45 minutes with Ika, the level of CHC found in the microsomal fraction was almost sevenfold greater than in S2 (Fig. 12D). In control experiments, the amount of CHC in P2 was about 1.6-fold greater than in S2 (Fig. 12D, Co). The same membranes used for CHC detection were also immunostained using an anti-α tubulin (Fig. 12C, lower blotting); the intensities of tubulin bands in S2 and P2 were similar with Ika and in the control.

Discussion

Data reported in this paper provide insights into the role of membrane retrieval in pollen tubes and the mechanisms of endocytic pathways in plants. The use of positively and negatively charged nanogold together with a specific type of fluorochrome allowed us to show different internalization events taking place in specific PM regions, such as the subapical and tip domains. EM observations and time-lapse experiments revealed endocytic pathways of the probes in great detail. The PM regions binding positively charged nanogold were reused in the secretory pathway through the Golgi apparatus, and were also consigned to the degradation pathway. PM domains binding negatively charged nanogold in the tip region were mostly relegated to the degradation pathway, although PM recycling at the very tip could not be excluded. Interestingly, endocytosis dissection using an inhibitor of clathrin-dependent endocytosis (Ika) revealed that clathrin-independent endocytosis might occur in pollen tubes. In fact, Ika inhibited the recycling of PM to SVs and the degradation pathway of negatively charged nanogold-binding PM, but the transport of positively charged nanogold to vacuoles and internalization of cell wall components were not affected. Evidence of internalization processes at the tip led us to consider a new hypothesis to explain vesicle accumulation at the apex, namely that endocytic vesicles might substantially contribute to V-shaped vesicle accumulation in addition to SVs.

Time-course experiments revealed distinct internalization events taking place in specific regions of the tube

In general, what we can deduce from analysis of positively and negatively charged nanogold internalization patterns is that the former is more abundant than the latter in the cell. The distribution pattern of positively charged nanogold involves organelles – such as cis, medial and trans elements of Golgi bodies, smooth ER and vacuoles – whereas negatively charged nanogold was only found in a limited number of vesicles in the tip region and in vacuoles. Sometimes, negatively charged gold particles were observed in vesicular-tubular elements related to the trans face of Golgi bodies, but not with cis or medial cisternae. The higher degree of internalization of positively charged nanogold occurs, although extra negative charges due to de-esterified pectins in the cell wall of the subapical regions compete with PM molecules to bind the probe.

In cells with high secretory activity, retrieval

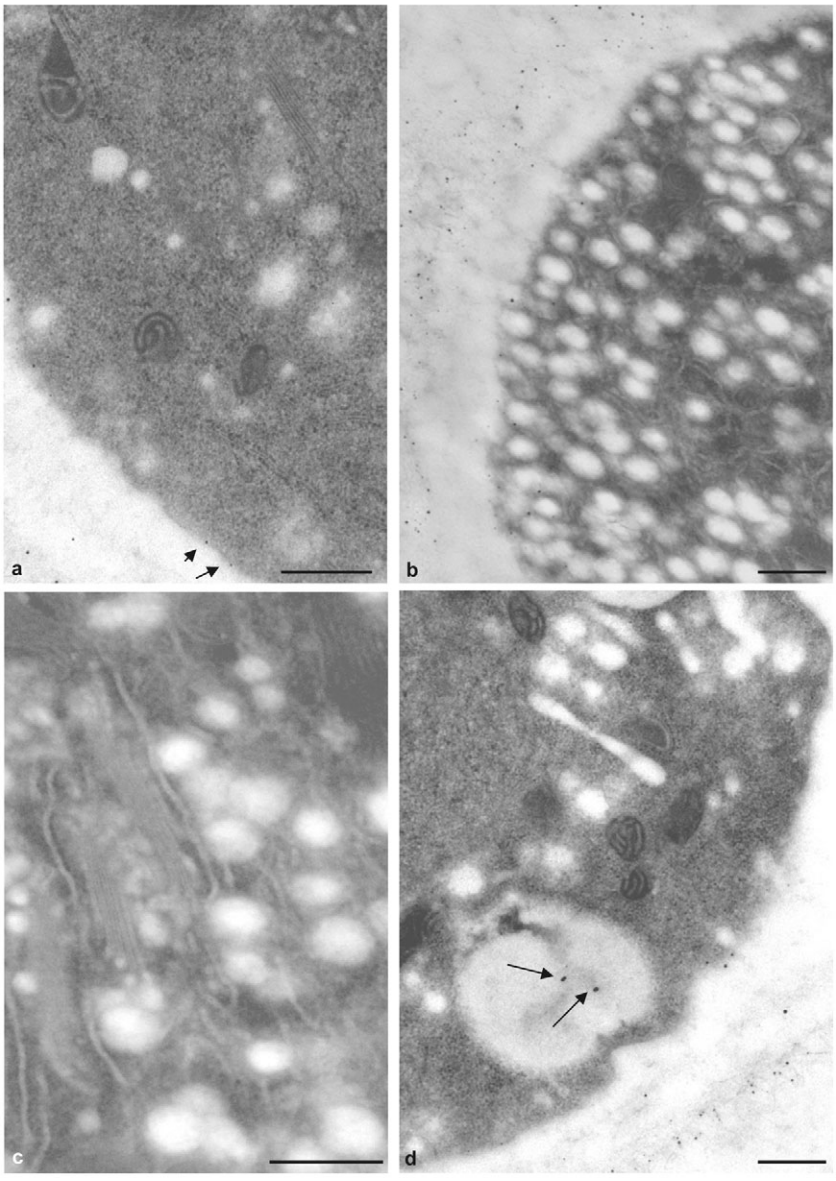

Fig. 7. Internalization of negatively charged nanogold for 2 hours. (a) Gold particles were seen associated with the PM (arrows) far from the tip. (b) In the tip region, only a few vesicles were stained. (c) Golgi bodies were not labelled. (d) Gold particles were observed in vacuoles after 2 hours of incubation (arrows). Bars, 0.5 μm.

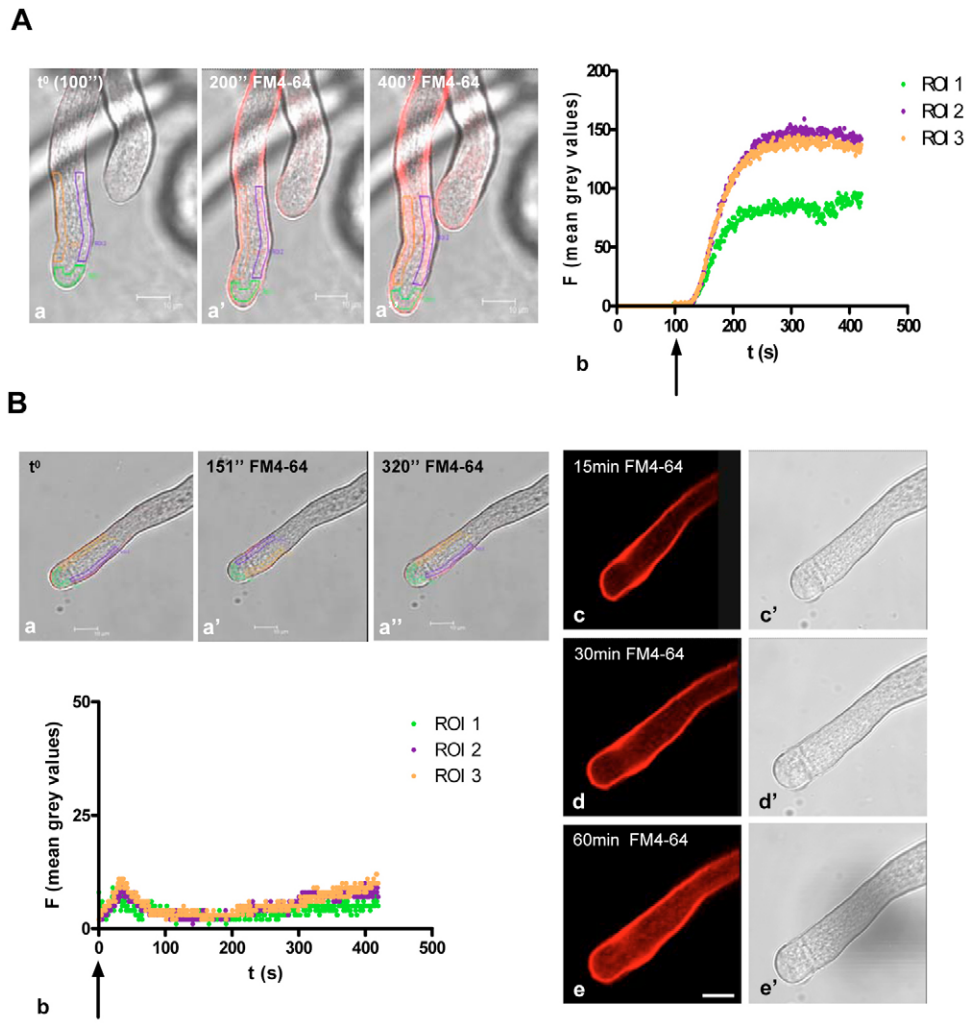

Fig. 8. Time-lapse experiments. (A) Control tubes. (Aa-Aa″) green ROI indicates the area measured in the tip region. Orange and violet ROI indicate the areas measured on the flanks of tubes. (Ab) Graph showing the mean fluorescence at the tip and in the subapical regions for 300 seconds. Arrow indicates the time of FM4-64 addition. (B) Ika-treated tubes. (Ba-Ba″) Coloured areas indicate regions in which fluorescence was measured (see above). (Bb) Graph showing mean fluorescence at the tip and in subapical regions for 400 seconds. Arrow indicates time of FM4-64 addition. (Bc-Be′) Medial plane images of the pollen tube 15-60 minutes after FM4-64 loading. Bars, 10 μm.

of excess PM secreted during exocytosis has been shown in animals and in plants. In neurons, internalized PM is trapped in synaptic vesicles at the tip and reused by the secretory pathway (Henkel et al., 1996); similarly, in pollen tubes, use of FM4-64 showed endocytosis of PM that then concentrated in the tip region, presumably only to be used again for exocytosis and to maintain membrane homeostasis in the cell (Parton et al., 2001). In our pulse-chase experiments, we

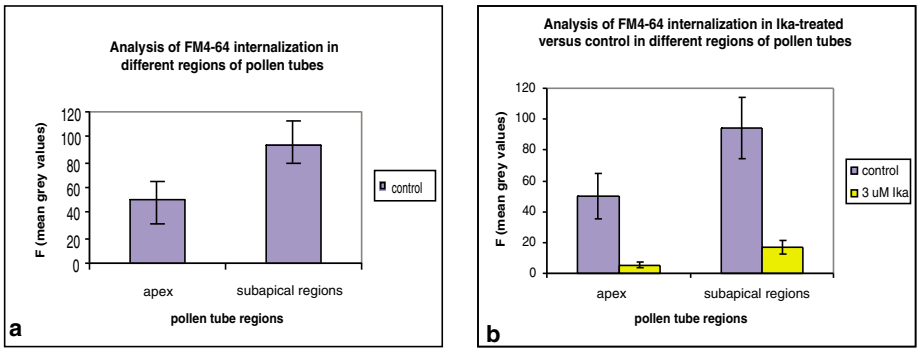

Fig. 9. Statistical analysis of quantitative FM4-64 uptake in the tip with respect to subapical regions of pollen tubes grown in control medium and with Ika. (a) Internalization of FM4-64 in flank regions was almost double that at the apex. (b) Quantitative analysis of FM4-64 internalization in two regions of the tube, in control medium and in the presence of Ika. (a,b) Error bars indicate 95% confidence intervals (n=6). t-test analysis of FM4-64 uptake in the presence and absence of Ika gave P values in control tubes and tubes incubated with Ika that indicated that inhibition of FM4-64 uptake was significant in the apical and subapical regions (control, P=0.01401; Ika, P=0.05294). Apical (Ika) versus apical (control): P=0.01149. Subapical (Ika) versus subapical (control): P=0.00142. For quantization, the last ten frames after reaching the steady state were considered in six independent experiments.

confirmed that internalized PM accumulated in the tip region, in which it formed a typical, dynamic V-shaped fluorescence accumulation (supplementary material Movie 2) that progressively disappeared as the pollen tube elongates and SVs fuse to the apex. Vacuole membranes were the final destination of FM4-64 because, 24 hours after the pulse, colocalization analysis showed that FM4-64 labelled the delimiting membrane of LysoSensor-stained organelles, therefore confirming the results of the pulse-chase experiments using charged nanogold. Positively and negatively charged nanogold were seen in MVBs and vacuoles in time-course and pulse-chase experiments, suggesting that degradative pathways were active in pollen tubes, even though a role as a secretory organelle has been recently ascribed to MVBs during defence reactions in barley (An et al., 2006).

The use of charged nanogold as a probe for ultrastructural observations provided insights into the pathways leading to membrane accumulation at the tip and relegation to vacuoles. We noticed that positively and negatively charged nanogold showed spatially distinct internalization patterns, because the former was internalized in the sides of tubes, presumably in the organelle-rich zone (up to 25 μm from the tip). This internalization pattern is in line with previous studies that showed coated vesicles 10-15 μm from the tip (Derksen et al., 1995) and suggested that a clathrin-dependent pathway occurs in this region (see below). In animal cells, internalized vesicles were first delivered to EEs, a sorting station of tubulo-vesicular structure that were characterized by specific sets of Rab-GTPases (Gruenberg, 2001; Zerial and McBride, 2001). In plant cells, a large number of Rab and SNARE homologues have been found in the *Arabidopsis* genome, but data on their localization and interactions are controversial (Geldner and Jurgens, 2006). ARA7, a Rab5 homologue, was suggested to be present on EEs involved in recycling the auxin efflux PIN1 to the PM (Ueda et al., 2004; Geldner, 2004). However, convincing evidence has been presented (Kotzer et al., 2004) that ARA7 localizes on late endosomes in tobacco leaf epidermal cells and is involved in vacuolar trafficking, because mutations that

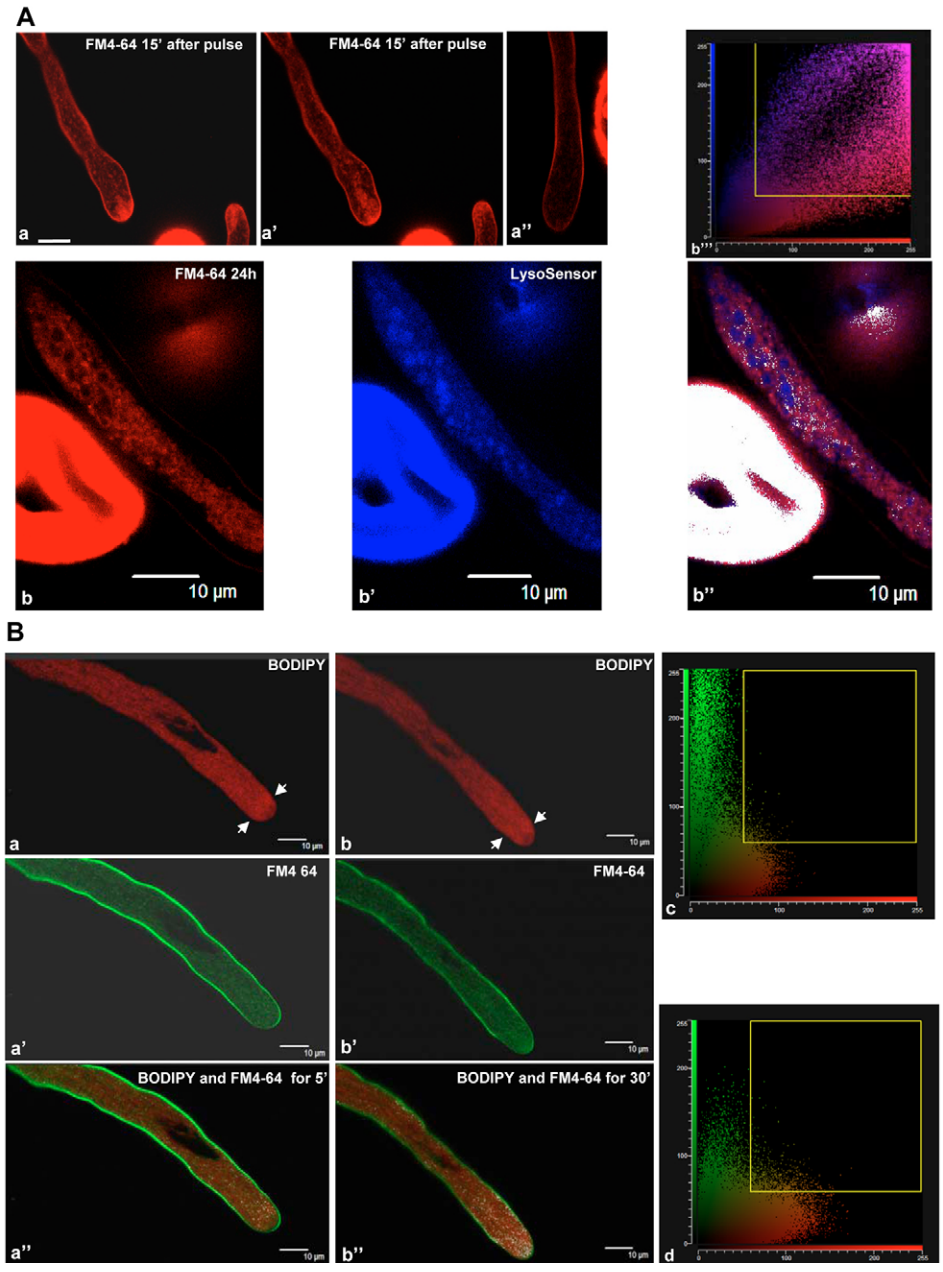

Fig. 10. Pulse-chase experiments using FM4-64, LysoSensor Blue and BODIPY TR-Ceramide. (A) Pulse-chase experiments using FM4-64. (Aa,Aa′) Internalized PM is accumulated in the tip region 15 minutes after the pulse. (Aa″) Five hours after the pulse, the staining in the apex was faint or absent. (Ab-Ab″) Pollen tube 24 hours after the pulse with FM4-64 (Ab); colocalization experiments using LysoSensor Blue (Ab′) showed that the probes overlap in the vacuolar membranes (Ab″). (Ab‴) Citofluogram that visualizes the frequency distribution of intensity in a 2D scatter plot. (B) Colocalization of FM4-64 with BODIPY-labelled membranes. (Ba,Bb) BODIPY TR-Ceramide-stained spots are distributed in the cytoplasm and are more concentrated in the tip region to form a collar-like structure (arrowheads) just behind the extreme tip at 5 (a) and 30 (b) minutes after the addition of FM4-64. (Ba′,Bb′) FM4-64 staining pattern after 5 (Ba′) and 30 (Bb′) minutes. (Ba″,Bb″) Colocalization analysis showing that probe staining overlaps in the collar-like structure and in the whole tip (white spots) after 5 and 30 minutes, respectively, after the addition of FM4-64. (Bc,Bd) Citofluograms that allow the distribution of intensity of green and red channels to be visualized in a 2D scatter plot referred to time-course analysis 5 and 30 minutes after FM4-64 addition, respectively. The ROIs select colocalized pixels. Bars, 10 μm.

impaired the function of ARA7 cause a delocalization of vacuolar markers.

Alternatively, colocalization of SNARE SYP41 and the vacuolar H^+ ATPase subunit 1a, but not ARA7, in compartments of the TGN suggested that the TGN can be regarded as an EE in plants (Dettmer et al., 2006). Compartments having a morphology similar to that described in animal EEs were not observed in the pollen tube; positively charged nanogold was seen immediately below the PM in vesicles that could be newly invaginated or EEs; in the latter case, they did not have tubulo-vesicular structure. Interestingly, the transport of positively charged nanogold involved other organelles, such as Golgi bodies. Positively charged nanogold was observed in vesicles associated with the trans face of Golgi apparatus, which is in line with the hypothesis that elements of the TGN could function as early endosomal compartments in plants (Dettmer et al., 2006; Geldner and Jurgens, 2006).

We were unable to unequivocally identify the compartments involved in this pathway, because specific anti-plant Rab antibodies were not available; however, the fact that TGN components were already labelled after 30 minutes indicates that they could be involved as an early endocytic compartment. Further studies using antibodies directed against different syntaxins could provide insights into the role of membranous compartments involved in degradation.

Stained vesicles associated with the rims of cis and medial cisternae of Golgi bodies revealed that this organelle also functions as a station for delivering internalized PM to the secretory pathway. In fact, after 2 hours of incubation, staining of the Golgi apparatus increased; quantitative analysis of several EM micrographs revealed that many vesicles in the clear zone contained gold particles, suggesting that the recycling of subapical PM domains into the secretory machinery is a major strategy to maintain cell membrane economy. These data were further confirmed using different kinds of probes. The Golgi-specific marker BODIPY TR-Ceramide and FM4-64 labelled membranes that were progressively colocalized in the apical collar-like structure and in whole the clear zone of the tube in time-lapse analysis.

After 2 hours, positively charged nanogold was also observed in tubules of smooth ER, dispersed in the apical region. Previous studies have not revealed endocytic markers in the smooth ER of plant cells. In pollen tubes, apical smooth ER has been postulated to play a main role in homeostasis of Ca^{2+}, because it functions as an internal Ca^{2+} store (Hepler et al., 2001); delivery of internalized membranes to smooth ER could play a role in maintaining the integrity of this compartment. Positively charged nanogold has been observed in internalizing vesicles containing fibrillar material, similar to cell wall components outside the protoplast, and we suggested that removing a

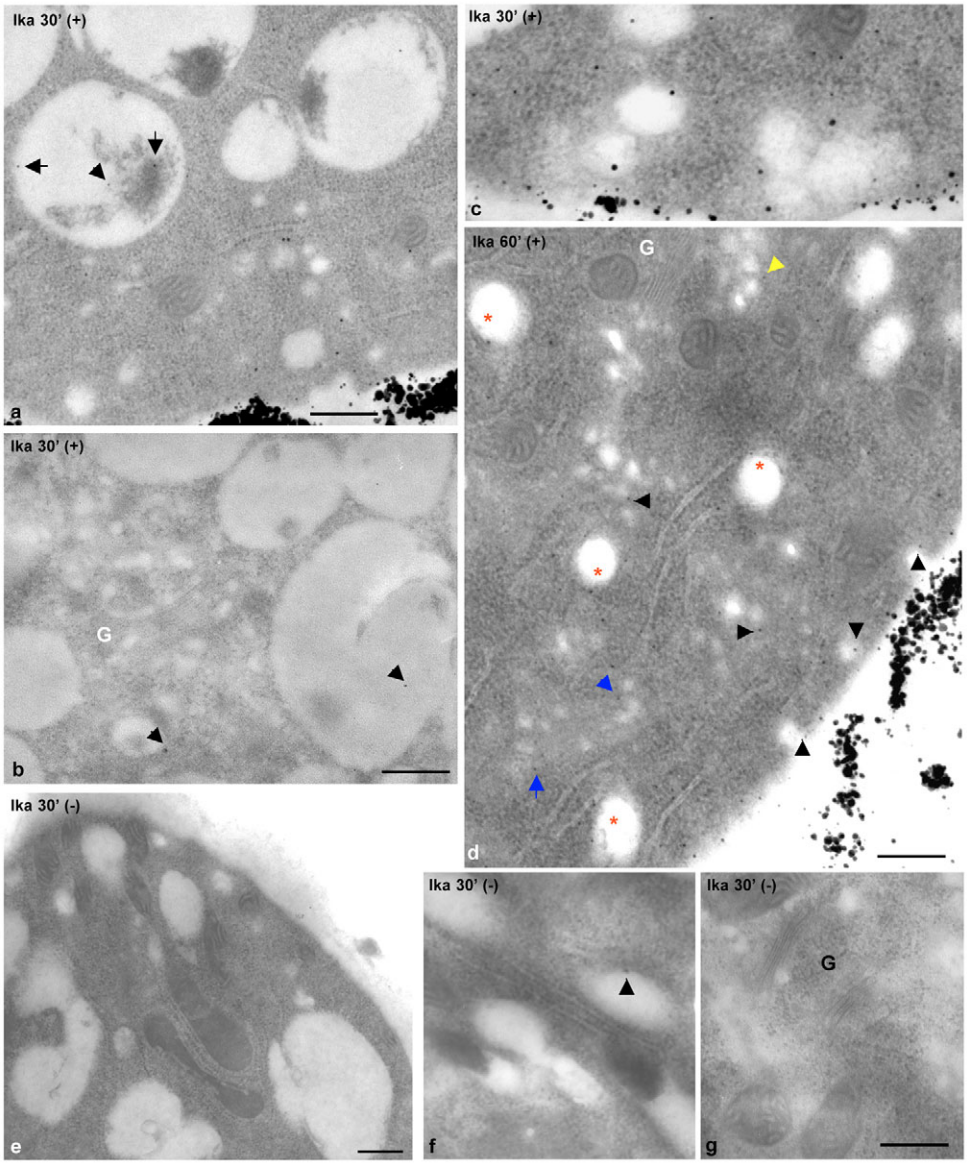

Fig. 11. Effect of Ika on positively and negatively charged nanogold internalization. (a,b) After 30 minutes incubation with Ika, positively charged nanogold was found in vacuoles (arrows and arrowheads), whereas the Golgi body (b, G) was not labelled. (c) Gold particles in vesicles containing fibrillar cell wall material after 30 minutes of incubation. (d) After 1 hour, positively charged nanogold was seen in small vesicles (black arrowheads). Large vesicles/endosomes were also labelled (asterisks). Golgi bodies in the picture only showed two gold particles (blue arrowheads), whereas one vesicle of the TGN was labelled (yellow arrowhead). (e-g) Negatively charged nanogold was not seen in vacuoles and was only sometimes observed in vesicles (f, arrowhead). Bars, 0.5 μm.

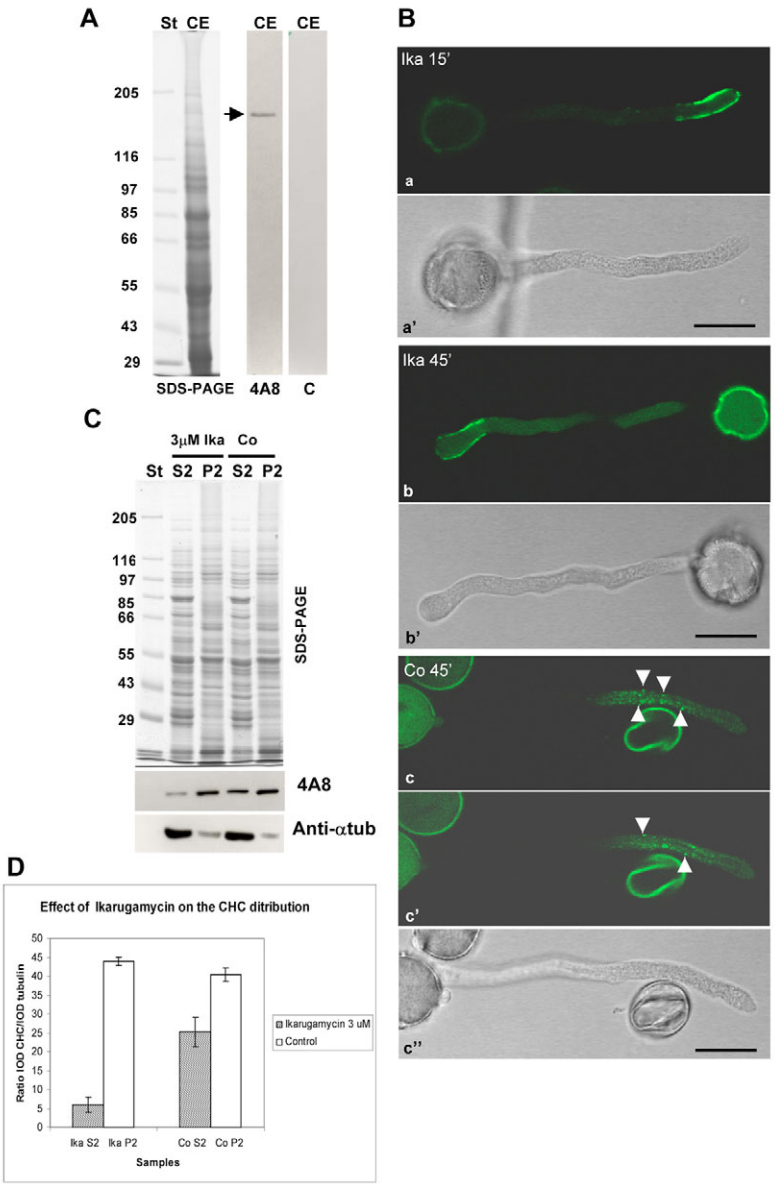

Fig. 12. Effect of Ika on the distribution of CHC. (A) The specificity of the 4A8 monoclonal antibody (Mab) was tested by SDS-PAGE and western blot of pollen tube crude extracts (CE). 4A8 antibody specifically recognized a 167 kDa polypeptide (lane 4A8, arrow). In the control (lane C) assay, the primary antibody was omitted. St, molecular-mass markers. (B) Immunostaining to reveal the effect of Ika on CHC distribution with 4A8 Mab. (Ba-Bb′) Medial sections of tubes (1 μm) treated with 3 μM Ika for 15 or 45 minutes showed increased association of CHC with the PM in the apical and subapical regions. (Bc,Bc′) In control (Co) experiments, 4A8 antibody gave punctate staining on the PM (arrowheads) and in the cytoplasm. Bars, 20 μm. (C) Cytoplasmic dissection with 3 μM Ika suggested that CHC was found in the microsomal fraction (P2) in preference to the soluble fraction (S2) (row 4A8). In the control microsome preparation, CHC appeared to be more equally distributed between P2 and S2 (row 4A8). Staining of membrane used for CHC detection with an anti-α tubulin antibody is also reported. (D) Densitometric analysis of anti-CHC western blot with Ika showed an integrated optical density (IOD) of CHC in P2 samples that was almost sixfold greater than that in S2, whereas, in the control experiments, it was only 1.6-fold greater than S2. Error bars indicate standard errors (n=3). 15 μg of proteins were loaded in each lane.

portion of cell wall could help to regulate wall plasticity during elongation, cooperating with cell wall loosening enzymes such as polygalacturonases and pectate lyases (Wen et al., 1999; Ren and Kermode, 2000). Internalization of pectins and arabinogalactan proteins is known in somatic plant cells, after which cell wall molecules are delivered to brefeldin A (BFA)-induced compartments, suggesting that they could also be recycled into the secretory pathway to limit de novo synthesis by the cell wall (Baluska et al., 2002; Baluska et al., 2005).

Negatively charged nanogold seemed to be internalized in the tip region of the tube, in which it appeared inside a few vesicles. Internalization events at the tip have been hypothesized in the pollen tube (Parton et al., 2001) and root hairs (Ovecka et al., 2005) on the basis of studies using FM dyes, but the authors could not discriminate the different pathways after tip internalization from those occurring in the subapical dome. Organelles such as the ER or cis, medial or trans cisternae of Golgi bodies were not seen to participate in negatively charged gold transport, suggesting that gold is not recycled into the secretory pathway through the Golgi apparatus. However, sometimes gold particles were observed in vesicles closely associated with the trans face of Golgi bodies, from which vesicles seemed to continue and to fuse with a compartment probably involved in degradation, because gold particles were released into its lumen, in which the pH was therefore presumably low. These observations again support the idea that the TGN could be a real meeting point between degradative and biosynthetic pathways in plants, and that negatively charged nanogold is basically sent to degradative compartments, although pulse-chase experiments suggest the possibility of limited recycling in the tip region. One hypothesis is that negatively charged nanogold could show a second exocytotic pathway involved in maintaining the necessary PM polarity/remodelling during tip growth. A mechanism of endocytosis at the tip was recently shown to be involved in recycling diacyl glycerol from the flanks to the tip of growing tobacco pollen tubes, thus regulating a differential lipid composition in the apical PM (Helling et al., 2006). Observing the movements of FM4-64-stained vesicles in the tip region, Parton and colleagues observed the apparent cycling of bright spots 10 μm from the apex back to the tip that could be related to internalization recycling of negatively charged nanogold in the apex (Parton et al., 2001).

Endocytosis has also been implicated in removing K^+ ion channels in order to accommodate changes in the surface area of guard cells following osmotic changes (Hurst et al., 2004; Meckel et al., 2004). Tip growing cells, such as pollen tubes, have a series of ion transporters that function in specific regions of the PM. Among these, Ca^{2+} channels and H^+ proton pumps in the tip and subapical regions, respectively, regulate actin filament organization and exocytosis (Hepler et al., 2001;

Lovy-Wheeler et al., 2006). The polarized localization of these complexes in different regions of the PM could require internalization/repositioning, explaining cycling of endocytic vesicles limited to the tip region.

Clathrin-dependent endocytosis was involved in internalization of PM to be recycled for secretion and participated in at least one degradation pathway

Ika is reported to inhibit clathrin-dependent endocytosis in mammalian cells without affecting internal trafficking (Hasumi et al., 1992; Luo et al., 2001). Immunostaining of pollen tubes with 4A8 monoclonal antibody suggested that Ika could inhibit the detachment of clathrin-coated pits from the PM in pollen tubes, because cells incubated with the drug showed an increased association of the CHC with the PM. This idea was further supported by experiments with microsome preparation from pollen tubes grown in the presence of Ika. In control tubes, the CHC appeared to be more equally distributed in the soluble and microsomal fraction, whereas, in treated tubes, association of CHC with P2 increased with respect to S2. Time-lapse experiments using FM4-64 showed that internalization was inhibited in the apical and subapical regions under these conditions. Nevertheless, coated vesicles have been reported in the tip region (Derksen et al., 1995) and the localization of CHC in the tip of lily pollen tubes (Blackbourn and Jackson, 1996) partly support our observations. In fact, in pollen tubes of *Lilium longiflorum*, the antibody stained the apical PM and also labelled apical and, with less intensity, subapical cytoplasm of the tube (Blackbourn and Jackson, 1996). Recently, Dhonukshe et al. reported data on the constitutive clathrin-dependent endocytosis of PIN efflux carriers in *Arabidopsis* protoplasts and suggested that clathrin-dependent internalization could be the predominant system in plants (Dhonukshe et al., 2007). However, the occurrence of clathrin-independent mechanisms in specialized cells such as pollen tubes could not be excluded. Our data on the presence of clathrin-independent pathways confirm data reported previously in which an accurate calculation of the retrieved membrane was performed (Derksen et al., 1995). This led to the conclusion that SVs deliver 430 μm^2 membrane/min, of which only 50 μm^2 is used for expansion, leaving an excess of 380 μm^2. The endocytic activity behind the tip, taken at its maximum of 225 μm^2/min, cannot retrieve a membrane surface of this size. Because, in this case only, the area delimited by coated pits or coated vesicles was considered, part of internalization could actually occur by clathrin-independent mechanisms.

Careful analysis of a certain number of cells after FM4-64 uptake showed that clathrin-dependent endocytosis could be involved in internalization of PM to be recycled to the secretory pathway, because most tubes (about 80%) observed after 30-60 minutes of incubation with the probe did not show the canonical V-shaped fluorescence in the tip region. Bright fluorescence of the PM behind the tip often suggested that the subapical region could be a point of substantial clathrin-dependent endocytosis. Statistical analysis of fluorescence with Ika compared to control showed that inhibition of internalization was greater in the flanks of the tube than at the tip (P=0.001 and 0.01, respectively). These results indicate the importance of recycling for tube elongation: in general, tube growth reduced but did not cease in the presence of Ika and it was quite common to observe a reduction of fluorescence in the tip PM during FM4-64 internalization in time-lapse experiments (supplementary material Movie 2), which suggested that tip growth proceeds at a reduced rate by de novo synthesis by the cell wall and PM. EM observation of positively charged nanogold internalized in the presence of Ika showed that, although the degradative pathway into vacuoles was not inhibited, staining of Golgi bodies was hardly observed. Only in one of the Golgi apparatus analyzed was gold labelling found. The others did not show any staining or they displayed labelled vesicles only in the TGN. Our data are in line with previous observations suggesting that clathrin-dependent endocytosis was involved in the removal of excess PM in growing root hairs and developing cell plates (Emons and Traas, 1986; Otegui and Stahelin, 2000; Baluska et al., 2005). Uptake of negatively charged nanogold at the tip seemed to be severely impaired, because vacuoles never contained gold particles and, in the cytoplasm, vesicles were only labelled sporadically. Because we did not make tip sections, we were unable to observe whether tip recycling was impaired as well. All this data clearly implies a function of clathrin-dependent endocytosis in removing excess secreted PM and PM receptors in pollen tubes, and might be a form of receptor downregulation. However, because the degradative pathway conveying positively charged nanogold to vacuoles was intact, it might also be worthwhile studying clathrin-independent internalization modes in pollen tubes.

Materials and Methods

Fluorescent probes and drugs

FM4-64 was dissolved in DMSO to a concentration of 16.4 mM and then diluted to 200 μM final concentration with distilled water. In time-lapse assays the probe was used at 1 μM in the culture medium. BODYPY TR-Ceramide and LysoSensor Blue DND-167 were dissolved in DMSO to a concentration of 1 mM. In colocalization experiments these probes were used at 4 μM and 2 μM, respectively. Ika stock solution in DMSO was 10 mM and was used at 3 μM final dilution in culture medium.

Pollen culture and pollen tube crude extracts

Nicotiana tabacum (L.) pollen was collected from plants grown in the Botanical Garden of Milan University, dehydrated by incubation for 12 hours in a box containing silica gel and then stored at –20°C. Before germination, pollen was hydrated in a humid chamber overnight. Pollen (2.5 mg/ml) was germinated in BK medium (Brewbaker and Kwack, 1963) containing 12% sucrose at 23±2°C. Pollen tubes were resuspended in two volumes of PEM buffer (100 mM Pipes pH 6.8, 5 mM EGTA, 1 mM $MgCl_2$, 1 mM DTT, 1 mM PMSF, 10 μg/ml TAME, 10 μg/ml leupeptin, 10 μg/ml pepstatin A, 4 μM aprotinin, 8 μM antipain) and homogenized on ice in a 2 ml Potter homogenizer. Laemmli sample buffer was added to the homogenate and the sample was boiled for 5 minutes. It was subsequently centrifuged at 4°C for 36 minutes at 20,627 ***g*** (15,000 rpm) in an ALC A21-C rotor. The resulting supernatant was collected as crude extract.

Pollen tube microsomes

Tobacco pollen tubes were grown for 2 hours as reported above. Then 3 μM Ika was added to the cell culture and samples were drawn after 45 minutes. As control, a sample of pollen tubes grown without Ika was obtained after 45 minutes. Pollen tubes were rinsed with 10 ml HEM buffer pH 7.4 (25 mM HEPES, 2 mM EGTA, 2 mM $MgCl_2$, 0.5 mM EDTA, 1 mM DTT, 1 mM PMSF, 10 μg/ml TAME, 10 μg/ml leupeptin, 10 μg/ml pepstatin A, 4 μM aprotinin, 8 μM antipain) containing 12% sucrose and centrifuged at 2000 rpm for 10 minutes at 10°C in a Beckmann JS13.1 rotor. Pollen tubes were then homogenized on ice in two volumes of HEM buffer containing 0.25 M sucrose as reported above. The homogenate was centrifuged at 572 ***g*** (2500 rpm) for 4 minutes at 4°C in an ALC A21-C rotor and the pellet was discarded. The supernatant was loaded onto a 0.5 M sucrose cushion (3 ml) in HEM buffer and centrifuged at 64,200 ***g*** (25,000 rpm) for 23 minutes at 4°C in a Beckmann SW 60 rotor. The membrane pellet (P2, microsomes) was resuspended in HEM buffer. Aliquots of P2 and supernatant (S2) were protein assayed (Bradford) using BSA as standard protein and then denatured for electrophoresis.

Electrophoresis and western blotting

Proteins were denatured and separated on 7% (crude extracts) or 8% (for the pollen tube microsomes) polyacrylamide gels following the method of Laemmli (Laemmli, 1970). Western blot was performed according to Towbin et al. (Towbin et al., 1979). 4A8 monoclonal antibody (Mab) against plant CHC (Blackbourn and Jackson, 1996), kindly provided by A. Jackson (Department of Biochemistry, University of Cambridge, UK), was used at final dilution of 1:1500. Anti-α tubulin Mab B-5-1-2 (Sigma) (1:3000). Detection of antibodies was performed as outlined in the Amersham ECL kit booklet. All gels and western blot images were scanned using Epson Expression 1680 PRO and Adobe Photoshop software. Quantification of CHC and tubulin levels was carried out by scanning immunoblots with a JX-330 colour image scanner (Sharp Electronics, Europe) into ImageMaster VDS Software (Pharmacia Biotech). Data were calculated as the ratio of arbitrary densitometric units of CHC immunoreactive bands normalized to values obtained for tubulin immunoreactive bands in the same immunoblots.

Nanogold internalization and EM

For time-course experiments, pollen (2.5 mg/ml, in 20 ml of culture medium) was allowed to germinate for about 1 hour before 30 nM of positively or negatively charged nanogold particles (Nanoprobes), resuspended in 200 μL of distilled water (MilliQ grade), were added; samples were obtained after 15 minutes, 30 minutes, 1 hour and 2 hours and processed for EM observation. Pollen tubes were incubated in fixing solution (50 mM HEPES pH 7.2, 5 mM EGTA, 1 mM $MgCl_2$, 12% sucrose, 2% formaldehyde, 0.2% glutaraldehyde) for 2 hours at room temperature and then stored at 4°C overnight. Samples were dehydrated with increasing concentrations of methanol. Infiltration and polymerization were done at –20°C, by using a CS-Auto cryo-substitution apparatus (Reichert Jung), according to the protocols supplied with the LR GOLD resin. 80 nm ultra-thin sections, obtained using a Reichert Jung Ultracut E microtome, were collected on gold grids. Positively and negatively charged nanogold were enhanced with QH silver (Nanoprobes) for 2 minutes as described by the manufacturer. Sections were then stained with 3% uranyl-acetate for 20 minutes and observed with Philips Morgagni electron microscopes at 80 kV. For endocytosis dissection, 3 μM final concentration of Ika was added to growing pollen tubes for 15 minutes before nanogold addition. Incubation with the probe was then carried out for 30 minutes or 1 hour before fixation.

In order to determine whether pollen tube growth was affected by charged nanogold or by Ika, five fields were considered for each sample and the lengths of pollen tubes at each time point were measured by TCS SP2 AOBS laser scanning microscope (CLSM) (Leica Microsystems Heidelberg GmbH, Germany). Pollen tube lengths were analyzed by the Excel programme.

For TEM characterization, a drop of gold nanoparticles (NP) dispersion was placed on formvar/carbon-coated nickel grids and dried in air. Grids were examined by an EFTEM LEO 912AB transmission electron microscope (Zeiss) working at 80 kV. Digital images were acquired by a CCD-BM/1K system. Diameter of NP was measured by Esivision software and average and standard deviation were calculated.

Time-lapse experiments and quantitative analysis

Time-lapse experiments were performed in live cells with the same CLSM equipped with an argon ion laser (458, 476, 488, 496, 514 nm excitation), three HeNe lasers (543, 594 and 633 nm excitation) and tunable emission wavelength collection. We excited FM4-64 using the 488 nm laser line and we imaged FM4-64 fluorescence between 625-665 nm (Bolte et al., 2004). A 40× Leica oil immersion plan apo (NA1.25) objective and a 2.7 zoom were used for all experiments. Bright-field imaging was performed with the transmitted light detector of the TCS SP2. To compare different experimental conditions, live data mode acquisitions were always performed with the same laser intensity and PMT settings. Viability of cells was assessed by recording pollen tube growth rate before the addition of the fluorochrome. Loading cells with the dye was achieved by direct addition of FM4-64 (1 μM) and time-course analysis of FM4-64 uptake was carried out with the Leica TCS SP2 software time-course option (1 frame/sec) for about 300 frames. Numbered images were converted to AVI file format using Adobe premiere software to view as video. Movies were then converted by using the QuickTime 7.1 programme and compressed by using the Sorenson option. Quantitative analysis of fluorochrome penetration was performed by Leica TCS SP2 software. Mean fluorescence intensity of the ROI was processed for statistical analysis (*t*-test) by Excel software.

Colocalization experiments

FM4-64–BodyPi and FM4-64–lisosensor colocalization experiments were carried out with a 63× oil immersion objective, zoom 1,7, pinhole 1 and a 1024×512 resolution. The 488 nm and the 594 nm laser lines were used to excite FM4-64 and BodyPi, respectively, and the fluorescence was collected in the same emission window (605-665 nm) acquiring FM4-64 and BodiPy images with the sequential scan mode of the Leica TCS SP2 software. LysoSensor was excited with the 315 and 364 UV laser lines and the emitted fluorescence collected between 400 and 490 nm. The scatter plots were generated by the Multicolor LCS Software.

Immunolabelling

For immunofluorescence microscopy, pollen was germinated in BK medium as reported for about 1 hour before the addition of Ika 3 μM final concentration. Antibody staining was performed according to Del Casino et al. (Del Casino et al., 1993). Optical sections (1 μm) and three-dimensional projections of specimens were obtained by the CLSM. A ×40 objective and BHS filterset were used for imaging.

We thank Anthony Jackson for providing the anti-CHC 4A8 monoclonal antibody. This work was supported by the PRIN project 2005, financed by the Italian Ministry of Education.

References

An, Q., Huckelhoven, R., Kogel, K.-H. and van Bel, E. (2006). Multivesicular bodies participate in a cell wall-associated defence response in barely leaves attacked by the pathogenic powder mildew fungus. *Cell. Microbiol.* **8**, 1009-1019.

Baluska, F., Hlavacka, A., Samaj, J., Palme, K., Robinson, D. G., Matoh, T., McCurdy, D., Menzel, D. and Volkmann, D. (2002). F-actin-dependent endocytosis of cell wall pectins in meristematic root cells. *Plant Physiol*. **130**, 422-431.

Baluska, F., Wojtaszek, P., Volkmann, D. and Barlow, P. (2003). The architecture of polarized cell growth: the unique status of elongating plant cells. *BioEssays* **25**, 569-576.

Baluska, F., Liners, F., Hlavacka, A., Schlicht, M., Van Cutsem, P., McCurdy, D. and Menzel, D. (2005). Cell wall pectins and Xyloglucans are internalized into dividing root cells and accumulate within cell plates during cytokinesis. *Protoplasma* **225**, 141-155.

Blackbourn, H. D. and Jackson, P. A. (1996). Plant clathrin heavy chain: sequence analysis and restricted localisation in growing pollen tubes. *J. Cell Sci*. **109**, 777-789.

Bolte, S., Talbot, C., Boutte, Y., Catrice, O., Read, N. D. and Satiat-Juenemaitre, B. (2004). FM-dyes as experimental probes for dissecting vesicle trafficking in living plant cells. *J. Microsc.* **214**, 159-173.

Bosch, M. and Hepler, P. K. (2005). Pectin methylesterases and pectin dynamics in pollen tubes. *Plant Cell* **17**, 3219-3226.

Brewbaker, J. L. and Kwack, B. H. (1963). The essential role of calcium ions in pollen germination and pollen tube growth. *Am. J. Bot*. **50**, 859-865.

Del Casino, C., Li, Y.-Q., Moscatelli, A., Scali, M., Tiezzi, A. and Cresti, M. (1993). Distribution of microtubules during the growth of tabacco pollen tubes. *Biol. Cell* **79**, 125-132.

Derksen, J., Rutten, T., Lichtscheidl, I. K., Dewin, A. H. N., Pierson, E. S. and Rongen, G. (1995). Quantitative analysis of the distribution of organelles in tobacco pollen tubes: implication for exocytosis and endocytosis. *Protoplasma* **188**, 267-276.

Dettmer, J., Hong-Hermesdorf, A., Stierhof, Y. D. and Schumacher, K. (2006). Vacuolar H^+ ATPase activity is required for endocytic and secretory trafficking in *Arabidopsis*. *Plant Cell* **18**, 715-730.

Dhonukshe, P., Aniento, F., Hwang, I., Robinson, D. G., Mravec, J., Stierhof, Y.-D. and Friml, J. (2007). Clathrin-mediated constitutive endocytosis of PIN auxin efflux carrier in *Arabidopsis*. *Curr. Biol.* **17**, 520-527.

Emons, A. M. C. and Traas, J. A. (1986). Coated pits and coated vesicles on the plasma membrane of plant cells. *Eur. J. Cell Biol*. **41**, 57-64.

Fowke, L. C., Tanchak, M. A. and Galway, M. E. (1991). Ultrastructural cytology of the endocytic pathways in plants. In *Endocytosis, Exocytosis and Vesicle Traffic in Plants* (ed. C. R. Hawes, J. O. D. Coleman and D. E. Evans), pp. 15-40. Cambridge: Cambridge University Press.

Geldner, N. (2004). The plant endosomal system – its structure and role in signal transduction and plant development. *Planta* **219**, 547-560.

Geldner, N. and Jurgens, G. (2006). Endocytosis in signalling and development. *Curr. Opin. Plant Biol.* **9**, 589-594.

Gruenberg, J. (2001). The endocytic pathway: a mosaic of domains. *Nat. Rev*. **2**, 721-730.

Hasumi, K., Shinohara, C., Naganuma, S. and Endo, A. (1992). Inhibition of the uptake of oxidazed low-density lipoprotein in macrophage J774 by the antibiotic ikarugamycin. *Eur. J. Biochem*. **205**, 841-846.

Helling, D., Possart, A., Cottier, S., Klahre, U. and Kost, B. (2006). Pollen tube tip growth depends on plasma membrane polarization mediated by tobacco PLC3 activity and endocytic membrane recycling. *Plant Cell* **18**, 3519-3534.

Henkel, A. W., Lubke, J. and Betz, W. J. (1996). FM1-43 dye ultrastructural localization in and release from frog motor nerve terminals. *Proc. Natl. Acad. Sci. USA* **93**, 1918-1923.

Hepler, P. K., Vidali, L. and Cheung, A. Y. (2001). Polarized cell growth in higher plants. *Annu. Rev. Cell Dev. Biol*. **17**, 159-187.

Heslop-Harrison, J. and Heslop-Harrison, Y. (1970). Evaluation of pollen viability by enzymatically induced fluorescence; intracellular hydrolysis of fluorescein diacetate. *Stain Technol*. **45**, 115-120.

Hillmer, S., Freundt, H. and Robinson, D. G. (1988). The partially coated reticulum and its relationship to the Golgi apparatus in higher plants. *Eur. J. Cell Biol*. **47**, 206-212.

Hurst, A. C., Meckel, T., Tayefeh, S., Thiel, G. and Homan, U. (2004). Trafficking of the potassium inward rectifier KAT1 in guard cell protoplasts of *Vicia faba*. *Plant J.* **37**, 391-397.

Kirkham, M., Fujiita, A., Chadda, R., Nixon, S. J., Kurzchalia, T. V., Sharma, D. K., Pagano, R. E., Hancock, J. F., Mayor, S. and Parton, R. G. (2005). Ultrastructural identification of uncoated caveolin-independent early endocytic vehicles. *J. Cell Biol.* **168**, 465-476.

Kost, B., Lemichez, E., Spielhofer, P., Hong, Y., Tolias, K., Carpenter, C. and Chua, N.-H. (1999). Rac homologues and compartmentalized phosphatidylinositol 4,5-biphosphate act in a common pathway to regulate pollen tube growth. *J. Cell Biol*. **19**, 317-330.

Kotzer, A., Brandizzi, F., Neumann, U., Paris, N., Moore, I. and Hawes, C. (2004). AtRabF2b (Ara7) acts on the vacuolar trafficking pathways in tobacco leaf epidermal cells. *J. Cell Sci.* **117**, 6377-6389.

Laemmli, U. K. (1970). Cleavage of structural proteins during the assembly of the head of bacteriophage T4. *Nature* **227**, 680-685.

Lovy-Wheeler, A., Kunkel, J. G., Allwood, E. G., Hussey, P. J. and Hepler, P. (2006). Oscillatory increases in alkalinity anticipate growth and may regulate actin dynamics in pollen tubes of lily. *Plant Cell* **18**, 2182-2193.

Low, P. S. and Chandra, S. (1994). Endocytosis in plants *Annu. Rev. Plant Physiol. Plant Mol. Biol.* **45**, 609-631.

Luo, T., Fredericksen, B. L., Hasumi, K., Endo, A. and Garcia, V. (2001). Human immunodeficiency virus type 1 Nef-induced CD4 cell surface downregulation is inhibited by ikarugamycin. *J. Virol.* **75**, 2488-2492.

Meckel, T., Hurst, A. C., Thiel, G. and Homann, U. (2004). Endocytosis against high turgor: intact guard cells of *Vicia faba* constitutively endocytose fluorescently labelled plasma membrane and GFP-tagged K^+ -channel KAT1. *Plant J.* **39**, 182-193.

Murphy, A. S., Bandyopadhyay, A., Holstein, S. E. and Peer, W. A. (2005). Endocytotic cycling of membrane proteins. *Annu. Rev. Plant Biol.* **56**, 221-251.

Nichols, B. J. and Lippincott-Schwartz, J. (2001). Endocytosis without clathrin coats. *Trends Cell Biol*. **11**, 406-412.

Otegui, M. and Stahelin, L. A. (2000). Syncytial-type cell plates: a novel kind of cell plate involved in endosperm cellularization of *Arabidopsis*. *Plant Cell* **12**, 933-947.

Ovecka, M., Lang, I., Baluska, F., Ismail, A., Illes, P. and Lichtscheidl, I. K. (2005). Endocytosis and vesicle trafficking during tip growth of root hairs. *Protoplasma* **226**, 39-54.

Parton, R. M., Fisher-Parton, S., Watahiki, M. K. and Trewavas. A. J. (2001). Dynamics of the apical vesicle accumulation and the rate of growth are related in individual pollen tubes. *J. Cell Sci*. **114**, 2685-2695.

Potocky, M., Elias, M., Profotova, B., Novotna, Z., Valentova, O. and Zarsky, V. (2003). Phosphatidic acid produced by phospholipase D is required for tabacco pollen tube growth. *Planta* **217**, 122-130.

Prescianotto-Baschong, C. and Riezman, H. (1998). Morphology of the yeast endocytic pathway. *Mol. Biol. Cell* **9**, 173-189.

Ren, C. W. and Kermode, A. R. (2000). An increase in pectin methylesterase activity accompanies dormancy breakage and germination of yellow cedar seeds. *Plant Physiol*. **124**, 231-242.

Steer, M. W. and Steer, J. L. (1989). Pollen tube tip growth. *New Phytol.* **111**, 323-358.

Tanchak, M. A., Griffing, L. R., Mersay, B. G. and Fowke, L. C. (1984). Endocytosis of cationized ferritin by coated vesicles of soybean protoplasts. *Planta* **162**, 481-486.

Towbin, H., Staehelin, T. and Gordon, J. (1979). Electrophoretic transfer of proteins from polyacrylamide gels to nitrocellulose sheets. Procedure and some applications. *Proc. Natl. Acad. Sci. USA* **76**, 4350-4354.

Ueda, T., Uemura, T., Sato, M. H. and Nakano, A. (2004). Functional differentiation of endosomes in *Arabidopsis* cells. *Plant J*. **40**, 783-789.

Wen, F. S., Zhu, Y. M. and Hawes, M. C. (1999). Effect of pectin methylesterase gene expression on pea root development. *Plant Cell* **11**, 1129-1140.

Zerial, M. and McBride, H. (2001). Rab proteins as membrane organizer. *Nat. Rev. Mol. Cell Biol.* **2**, 107-117.

Journal of Cell Science